energies

MDPI

Review

Comprehensive Review of Methods and Instruments for Photovoltaic–Thermoelectric Generator Hybrid System Characterization

Petru Adrian Cotfas * and Daniel Tudor Cotfas

Department of Electronics and Computers, Faculty of Electrical Engineering and Computer Science, Transilvania University of Brasov, 500036 Brasov, Romania; dtcotfas@unitbv.ro

* Correspondence: pcotfas@unitbv.ro

Received: 16 October 2020; Accepted: 13 November 2020; Published: 19 November 2020

Abstract: Finding new sustainable energy sources or improving the efficiencies of the existing ones represents a very important research and development direction. The hybridization approach is one solution for increasing the efficiency of the existing energy sources. In the case of photovoltaic technology, the hybridization of the photovoltaic panels (PV) with thermoelectric generators (TEGs) has become a more interesting solution for the research community in the last decade. Thus, a comprehensive review of the characterization methods and instruments used in PV-TEG hybrid system study represents the objective of this work. PV and TEG equivalent circuits are presented. The instruments and software applications used for the measurements and simulations are presented and analyzed. The analysis of the literature reveals that there are many papers that offer partial or no information about the instruments used or about the measurement quality (accuracies, uncertainties, etc.). In hybrid system modeling, the preferred software applications are MATLAB (MathWorks, Natick, MA, USA) and COMSOL Multiphysics (Comsol, Burlington, MA, USA), while for experimental studies based on computers, LabVIEW (NI, Austin, TX, USA) is preferred. This review work could be interesting for researchers and engineers who are interested in finding solutions for characterizing or monitoring hybrid system components, but it is not limited to these.

Keywords: hybrid system; thermoelectric generator; photovoltaic; I–V characteristics; Internet of Things

1. Introduction

Today, energy generation from renewable energy sources (RES) is very important for humankind, replacing the used fossil energy sources. RES have the advantages of inexhaustibility and low pollution but have the disadvantages of intermittency and relatively high upfront costs. Therefore, finding new RES or better solutions to improve current RES performance represents the goal of the research community and industry. According to the report of REN21 [1], the target of the EU is to have at least 32% of the energy used coming from RES by 2030. One direction for improving the efficiency of RES is hybridization. There are many solutions for implementing RES hybridization; each of them comes with advantages and disadvantages.

One of the most important RES is solar photovoltaic energy sources. In order to convert solar energy into electrical energy, photovoltaic panels are used. Several technologies are used to produce photovoltaic (PV) cells and modules, with different efficiencies. The efficiencies of the currently used PVs types are presented in [2]. For single-junction terrestrial cells or modules, the maximum efficiencies reported are 29.1% for PV cells based on III-V materials and 26.7% for silicon photovoltaic panels, while for multiple-junction cells or modules under standard test conditions, the maximum efficiency of 38.8% is reported for five junction cells, while under concentrated light, the maximum efficiency of

47.1% is reported for six-junction cells [2]. The efficiencies of all the above-mentioned cells are affected by the working conditions. One of the most important parameters that affects the PVs' performance is their working temperature. Cotfas et al. [3] presents a study regarding the influence of temperature on four commercial PVs: three single-junction and one three-junction. They found that the maximum power at 1000 W/m^2 for mSi decreases by 0.47%/°C. In real working conditions, the temperatures of the PV modules can reach values of 70–80 °C. In this case, the maximum power can decrease by more than 17%. Therefore, the reduction in the working temperature of the PVs represents an important direction for research. In order to cool the PVs, many solutions are proposed in the specialist literature. There are passive or active solutions. One passive solution is presented in [4], based on aluminum fins placed on the back of the PV panel. The gain in the PV power yield is 5%. Other passive solutions, numerically tested, are presented in [5]. The proposed solutions are based on changing the PV panel frame material, PV panel frame geometry, and front PV panel surface geometry. The last one showed the highest influence, decreasing the temperature of the PV panel by 4 °C [5].

Another solution for cooling the PV panels is based on water by combining the PV panels with a solar thermal collector, resulting a hybrid photovoltaic thermal (PVT) system [6]. There are PVTs with natural or forced water circulation. The advantage of the PVT is that it increases the efficiency of the PV electrical energy generation due to a PV temperature decrease and adds thermal energy generation. Based on the same idea, hybrid systems (HSs) with a PV-TEM (thermoelectric module) structure became interesting for researchers. The PV-TEM can be used in two ways. In the first, the TEM is used as an electrical co-generator component of an HS. In this case, the TEM works based on the Seebeck effect, extracting heat from the PV panels and generating electrical energy and acts as a thermoelectric generator (TEG). The second way is based on the Peltier effect when the TEM works as a thermoelectric cooler (TEC). In this case, a current is injected through the TEC, creating a temperature difference between its sides that cools the PV panels. The current is provided by an additional PV panel [7]. In both cases, a heat sink should be used in order to dissipate the heat from the second side of the TEG or TEC. Based on this, a PV-TEG-T appears as a cooling solution for PVs and thermal energy generation. Even if the TEG presents many advantages such as direct energy conversion, no moving parts, a long lifespan and scalability [8], the high price for the module and the very low efficiency decrease the usability of the TEGs on a large scale. The actual interest of the industry is creating a climate of decreasing prices per module through the finding of new, less-expensive materials that are also more environmentally friendly. Therefore, combining the PV with the TEG is becoming more feasible and more interesting for researchers and industry. Such interest is also proven by the number of review papers that have been published in the last three years, having, as the subject, the TEG as an individual component or as a component of the HSs. Different aspects are considered for the review papers, such as the technologies, materials and applications for using TEGs [9], the structure and geometry optimization of the TEG [10], experimental studies on thermoelectric figure-of-merit improvement [11], thermal configurations for solar applications [12], improving photovoltaic or HS system performance by using TEGs, HSs such as PV/TEG [13,14] and PV/T [15,16].

In order to determine the performance of the studied HSs or their components separately, researchers have used a large variety of methods and instruments. Analyzing the review papers, one can notice that there is no review carried out on the methods and instruments for HS component characterization. Therefore, this paper is focused on reviewing and analyzing the instruments and methods used for PV and TEG characterization as components of an HS or as independent components. The considered papers are limited to the ones that offer information about the methods and instruments used for HS component characterization (software for modeling and simulation and equipment or apparatus used for experimental studies), with some exceptions that allow defining the context of the paper. The rest of the paper is organized in four sections. Section 2 presents the solutions proposed for implementing the HS based on PV and TEM. In Section 3, the models used for the HS components are presented. The characterization methods and instruments used for HSs and their components are reviewed in Section 4. Section 5, the last one, is focused on the discussion and conclusions.

2. HS Structures

Different HS designs have been proposed for improving the efficiency of the PV components or of the system through TEG cogeneration. Under concentrated light, different structures were analyzed in [17], while in this section, the most used structures of the HS systems based on PV and TEG in normal and concentrated light are briefly reviewed.

The first structure considered in this paper is the PV-TEC. The TEC has the goal of cooling down the PV in order to increase the efficiency of the PV. The most used structure is a sandwich structure called directly coupled, as shown in Figure 1 [7]. The TEC element is placed between the PV and a heat sink. The cold side of the TEC is in contact with the PV, and its hot side is connected to the heat sink. The power supply for the TEC is provided by a second panel. By using the second panel and the TEC, the price cost of the system is increased. Based on the economic analysis presented in [7], the cost of the system increases by 6%.

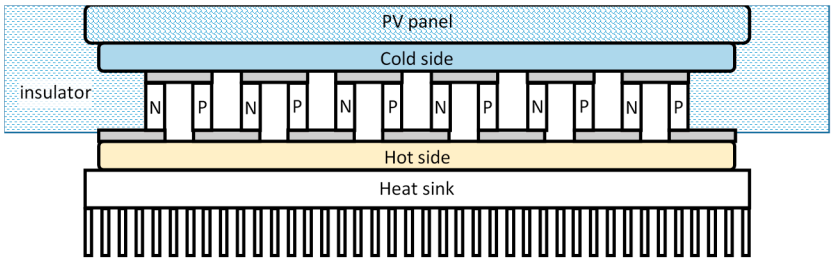

Figure 1. Photovoltaic–thermoelectric cooler (PV-TEC) structure.

The second structure is the PV-TEG (Figure 2). The TEG is used for cooling the PV by absorbing the heat from the PV, converting a part to electricity (electrical cogeneration) and transferring the rest of the heat to a heat sink. The advantage of this structure is the electrical cogeneration of the TEG, but the cooling efficiency is less than in the PV-TEC configuration. The heat sink could be passive (aluminum heat sink) or active (water [18,19] or nanofluids [20]).

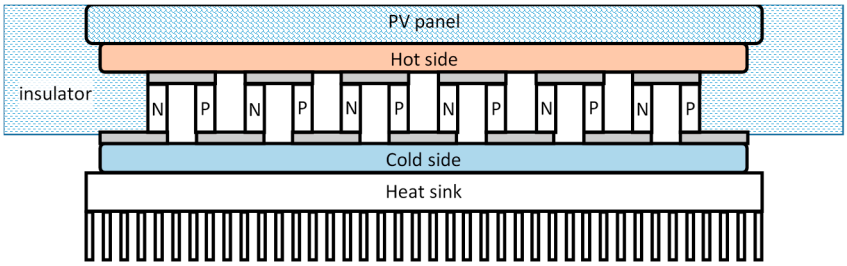

Figure 2. PV–thermoelectric generator (PV-TEG) structure.

The third one is presented in Figure 3, being formed from three active components also placed in a sandwich structure (PV-TEG-T). In this structure, the heat sink is replaced with a thermal collector in order to add thermal energy generation besides the electrical generation of the entire HS.

There are structures proposed in the literature that are indirectly coupled, supposed to have a distributed structure or mixed. Therefore, the fourth structure is PV-TEG distributed, shown in Figure 4. In fact, this structure is a mixed one that involves heat pipes or a micro-channel heat pipe (MCHP) system composed of two parts: an evaporator part that is directly coupled with the PV, extracting waste heat from the PV, and a condenser part that is directly coupled with the TEG, conducting the heat to the hot side of the TEG [21–23].

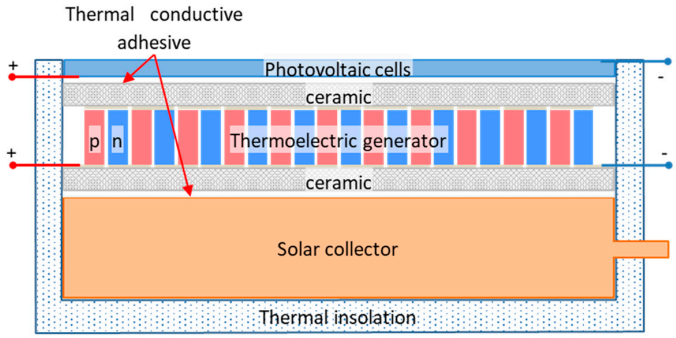

Figure 3. PV-TEG-T structure.

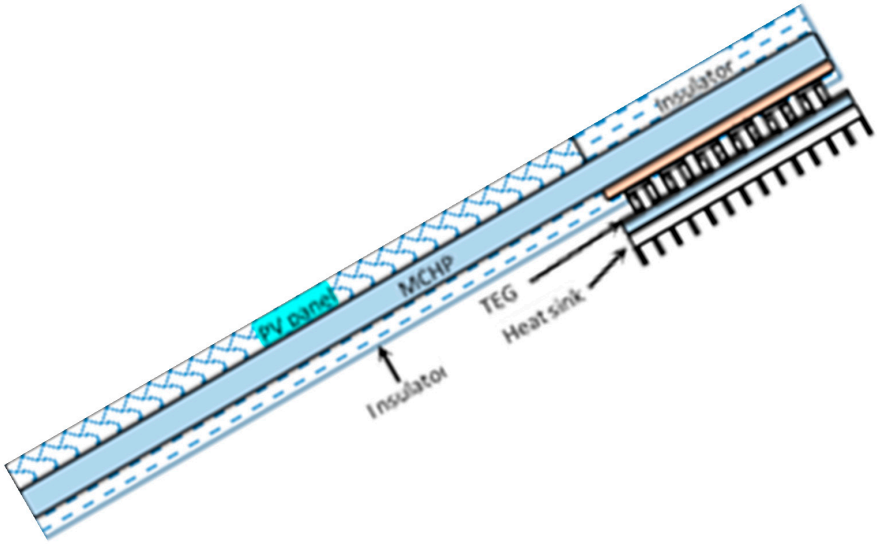

Figure 4. PV-TEG structure with micro-channel heat pipe (MCHP).

The fifth structure that is considered in the specialist literature is based on the separation of the light spectrum into two parts, long and short wavelengths, using a beam splitter (BS) in concentrated sunlight, as shown in Figure 5. The shorter wavelengths are focused to the PVs, and the longer wavelengths are focused on the TEGs.

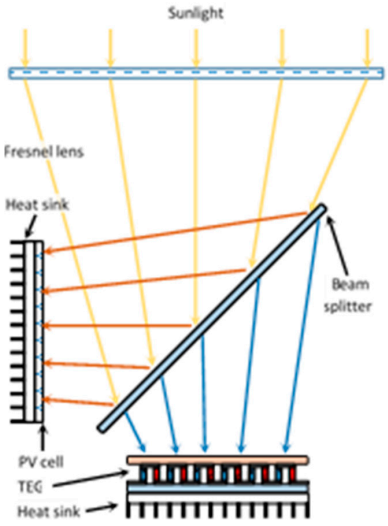

Figure 5. PV-TEG indirectly coupled structure with beam splitter.

3. HS Component Models

3.1. PV Models

In order to characterize the HS system, its components should be characterized separately or together. The most used method for PV characterization is based on measuring its I-V characteristics (under light or in dark conditions). Based on the I–V characteristics, the most important parameters can be determined based on different methods.

The models used for PV characterization are the one-diode model (one-diode), the two-diode model (two-diode) and the less utilized, three-diode model (three-diode). The internal structures of the three PV models are shown in Figure 6.

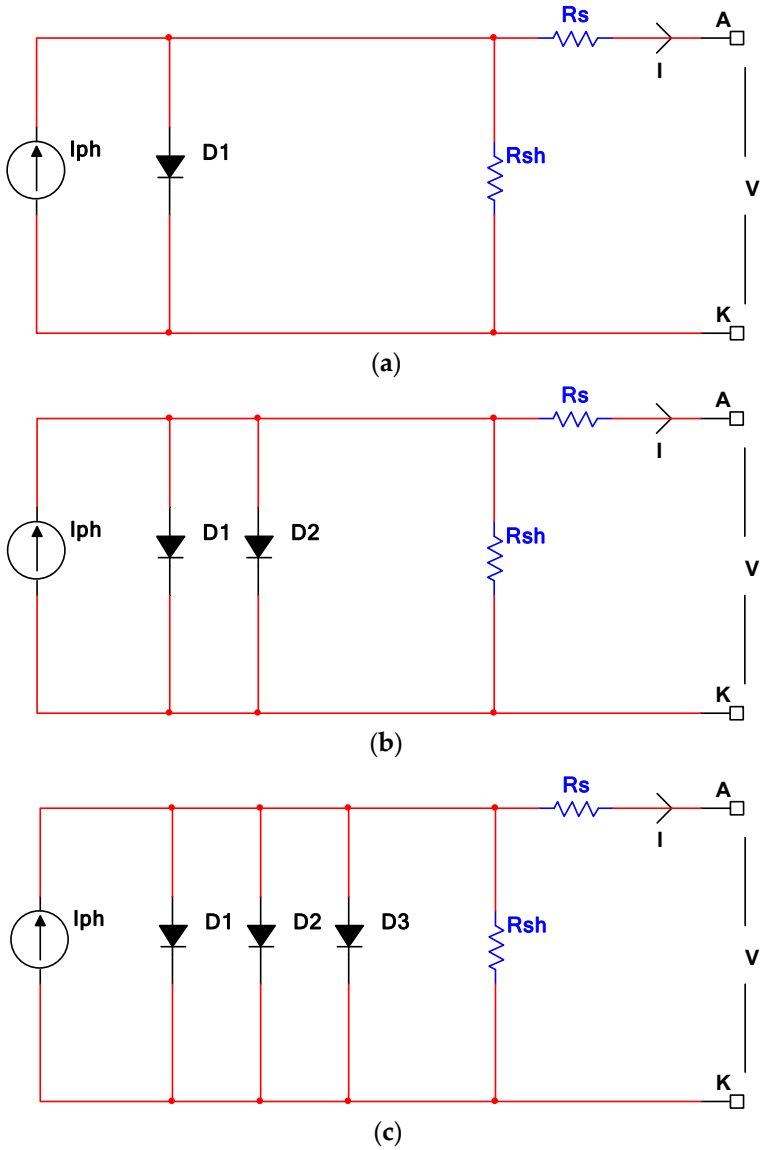

Figure 6. PV models: (**a**) one-diode model; (**b**) two-diode model; (**c**) three-diode model.

The equations that describe the three models are:

- One-diode model:

$$I = I_{ph} - I_0\left(e^{\frac{q(V+IR_s)}{nkT}} - 1\right) - \frac{V + IR_s}{R_{sh}} \quad (1)$$

- Two-diode model:

$$I = I_{ph} - I_{01}\left(e^{\frac{q(V+IR_s)}{n_1 kT}} - 1\right) - I_{02}\left(e^{\frac{q(V+IR_s)}{n_2 kT}} - 1\right) - \frac{V + IR_s}{R_{sh}} \quad (2)$$

- Three-diode model:

$$I = I_{ph} - I_{01}\left(e^{\frac{q(V+IR_s)}{n_1 kT}} - 1\right) - I_{02}\left(e^{\frac{q(V+IR_s)}{n_2 kT}} - 1\right) - I_{03}\left(e^{\frac{q(V+IR_s)}{n_3 kT}} - 1\right) - \frac{V + IR_s}{R_{sh}} \quad (3)$$

where I and V are the current and voltage generated by the PV, I_{ph} is the photogenerated current, I_0 is the reverse saturation current, q is the elementary electrical charge, R_s and R_{sh} are the series and shunt resistances, n is the ideality factor of the diode, k is the Boltzmann constant and T is the temperature. The 1, 2 and 3 indexes relate the diffusion, the generation–recombination and the thermionic mechanisms, respectively.

The efficiency of the PV is calculated based on the following Equation (4):

$$\eta_{PV} = \frac{P_{max}}{A \times G} = \frac{V_{max} \cdot I_{max}}{A \times G} \quad (4)$$

where P_{max} is the maximum power generated by the PV, I_{mpp} and V_{mpp} are the current and voltage generated by the PV at the maximum power point, A is the PV area and G is the incident radiation.

In Figure 7, the thermal model is added beside the one-diode electrical model. The model components are P_{th}, the current source that models the radiation absorbed and converted to heat, and the power dissipated on R_s and R_{sh}; R_{th}, the thermal resistance; C_{th}, the lumped heat capacitance of the PV; E_Rs, which is a voltage source that models the variation of the R_s depending on the temperature; T_{pv}, the PV temperature; and I_d, the current source that models the current through the diode [24].

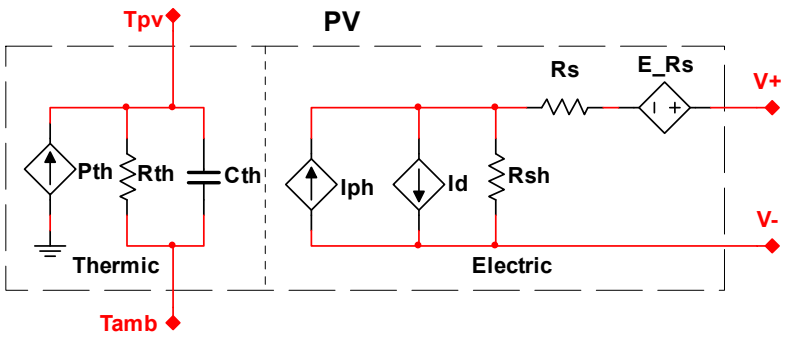

Figure 7. PV model—electrical and thermal parts [24].

3.2. TEG Models

The TEG characterization methods are based on measuring the V_{OC}, the output voltage for a defined load, and the output voltage for maximum power generation or on I–V characteristics, but depend on the temperature difference between the hot and cold sides of the TEG.

The behavior of the TEG is described through the following Equations (5) and (6) [25]:

$$V_{TEG} = \alpha \times \Delta T = N \cdot \left(\alpha_n - \alpha_p\right) \times \Delta T \quad (5)$$

$$I_{TEG} = \frac{\alpha \times \Delta T}{R_{TEG} + R_L} \quad (6)$$

where V_{TEG} and I_{TEG} are the voltage and current generated by the TEG; α is the Seebeck coefficient of the module; $\alpha = N(\alpha_n - \alpha_p)$, with α_n and α_p being the Seebeck coefficients of the n- and p-type semiconductors of a single thermocouple and N being the number of TEG thermocouples; $\Delta T = T_h - T_c$ is the temperature difference between the temperatures of the hot side (T_h) and the cold side (T_c) of the TEG; $R_{TEG} = NR_0$ is the internal resistance of the TEG; R_0 is the resistance of a single thermocouple; and R_L is the load resistance applied to the TEG.

The efficiency of the TEG is calculated through Equation (7) [26]:

$$\eta_{TEG} = \frac{W_{max}}{Q_h} = \frac{\Delta T}{T_h} \frac{\sqrt{1+ZT}-1}{\sqrt{1+ZT}+\frac{T_c}{T_h}} \tag{7}$$

$$Z = \frac{\left(\alpha_p - \alpha_n\right)^2}{\left(\left(k_p \times \rho_p\right)^{1/2} + \left(k_n \times \rho_n\right)^{1/2}\right)^2} \tag{8}$$

where W_{max} is the maximum electrical energy produced by the TEG; Q_h is the thermal energy received on the TEG hot side; α_p, α_n, k_p, k_n, ρ_p and ρ_n are the Seebeck coefficients, thermal conductivities and electrical resistivities of the p and n materials, respectively; $T = (T_h + T_c)/2$ is the average temperature; and Z is the thermoelectric figure of merit of the TEG [27]. The ZT product is known as the dimensionless figure of merit [27], and it is used as the characterization parameter for the TEG. The current TEGs have a ZT around 1. The goal of researchers is to increase this parameter to 2 or larger, in order to increase the efficiency of the TEGs [8].

ZT can be calculated based on the following Equation (9) [28,29]:

$$ZT = \frac{\alpha^2}{k \times \rho} T \tag{9}$$

where k is the mean thermal conductivity and ρ is the mean electrical resistivity. These parameters are temperature dependent [28].

Another parameter used to characterize the TEG performance is the power factor PF, which is defined by Equation (10) [29]:

$$PF = \frac{\alpha^2}{\rho} \tag{10}$$

The electrical models of the TEG are presented in Figure 8.

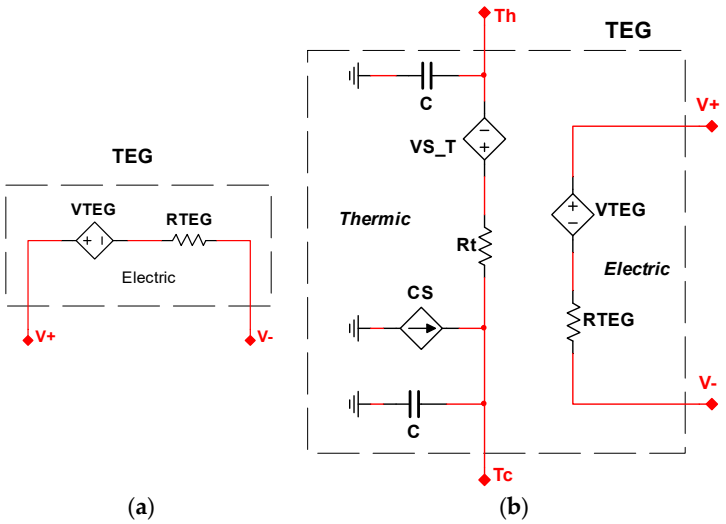

Figure 8. TEG models: (**a**) only electrical part [26]; (**b**) electric and thermal parts [24].

In Figure 8, the thermal model is included, consisting of VS_T, the voltage source that models the Peltier cooling and heating on the corresponding sides; *CS*, the current source that models the Joule effect through the TEG; R_t, the resistance that models the thermal resistance of the TEG; and *C*, the capacitors that model the lumped heat capacitance of the ceramic plates of the TEG [24,30].

For better results, models based on the energy conservation law for each layer that composes the TEG have been developed and proposed in the literature [31]. Such models are based on solving differential equations that characterize each contact surface of the TEG components.

4. HS Characterization

Studies of the PV-TEG hybrid systems are based on numerical modeling and simulation and on experimental measurements.

In order to characterize the HS components, their working parameters should be measured, such as the currents, voltages, temperatures for different applied loads and environmental testing conditions. In order to obtain the HS system behavioral responses working in different conditions and configurations, different measurement instruments are used. From the theoretical point of view, different software applications are used for modeling and simulation. According to Turcotte et al. [32], the software used for HS design is grouped into four categories: pre-feasibility tools, sizing tools, simulation tools and open architecture research tools. Sinha et al. [33] reviewed 19 pieces of software dedicated to hybrid system design, but few of them are used in the design, and fewer are used for the characterization of the PV-TEG HS.

4.1. Numerical Studies

In this section, papers that are mainly focused on modeling and simulation are presented, considering the methods used for mathematical equation solving and the software used for modeling and simulation. Some of the cited papers also include the confirmation of the simulation results with experimental ones.

An ideal model of a directly coupling PV-TEG HS was studied in [34]. The proposed model is based on the following equation:

$$\eta_{PV}(G,\ T_{PV}) = \eta_{PV}(G,\ 25) \times (1 + \alpha \times (T_{PV} - 25)) \tag{11}$$

$$\eta_{PV}(G,\ 25) = a_1 + a_2 \times G + a_3 \times ln(G) \tag{12}$$

$$T_{PV} = T_a + c \times G \tag{13}$$

$$\eta_{TE} = \frac{T_{PV} - T_a}{T_{PV}} \frac{\sqrt{1 + ZT} - 1}{\sqrt{1 + ZT} + \frac{T_a}{T_{PV}}} \tag{14}$$

$$T = \frac{1}{2}(T_{PV} + T_a) = T_a + \frac{1}{2} c \times G \tag{15}$$

where $\eta_{PV}(G,\ T_{PV})$ is the PV efficiency at the irradiance level *G* and temperature T_{PV}; $\eta_{PV}(G,\ 25)$ is the PV efficiency at the irradiance level *G* and temperature 25 °C; a_1, a_2 and a_3 are PV-specific parameters that can be found from the PV datasheet or through experiments; T_a is the ambient temperature; *c* is a proportional coefficient that is dependent on the system installation conditions; is the TEG efficiency at the temperature difference $T_{PV} - T_a$; and *T* is the average working temperature. Sark found that the contribution of the TEGs to the overall annual energy yield of the HS is between 11.0% (in Utrecht) and 14.7% (in Malaga). In real conditions, Sark estimates that due to the different losses, the contribution of the TEGs to the overall HS annual energy yield could be 10% less.

A simulation study was carried out by Koushik et al. in [35]. This study was based on a PV-TEG directly coupled HS structure, introducing a new layer of CO_2 gas, with the goal of increasing the heat absorption from the solar irradiation through the greenhouse effect. The gas layer was placed between the PV and TEG. The irradiance not utilized by the PV was absorbed by the CO_2 and was

converted to heat. For simulation, the MATLAB-Simulink software package was used. For the PV component, the one-diode model was chosen, and the PV model from the Simulink library was used. Monocrystalline and multijunction PV arrays were studied. The multijunction PVs were implemented as four subcells connected in series. Through series and parallel cell connections, 50 and 80 Wp power rates were modeled for the monocrystalline and multijunction panels, respectively. Through this study, it was shown that the HS maximum power density increased by 58.09% and 36.68% for the monocrystalline and multijunction panels, respectively, in comparison with the PV component alone.

An HS with a directly coupled structure was proposed in [36] for application for precision agriculture. In order to ensure enough energy for 24 h/day, a battery bank was included in the HS. A MATLAB-Simulink model of the HS with a battery bank was developed and analyzed by the authors, as is shown in Figure 9. An interesting result is presented in this paper, based on real measurements. It was observed that there is also a difference between the PV and ambient temperatures during the night that can be used by the TEG to generate consistent energy throughout the day. The day energy generation by the HS components is 1110.88 Wh by the PVs and 37.6 Wh by the TEGs. This means that the TEGs, as HS components, increase the PV power production by 3.4%.

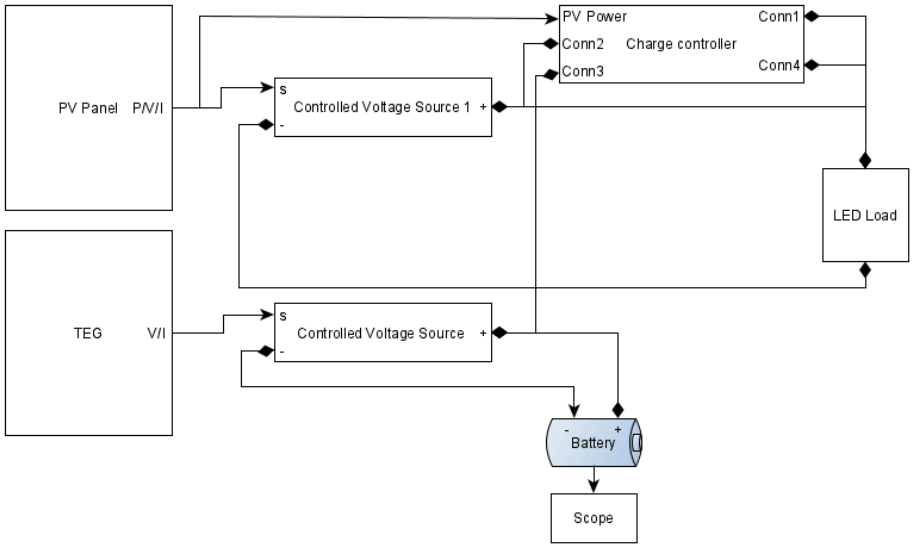

Figure 9. Hybrid system (HS) with battery bank model [36].

The HS for space applications is presented in [37]. The directly coupled structure is used with a special heatsink with an aluminum honeycomb structure. The finite volume method was used for modeling the heat transfer through the HS layers. Seven segments were identified in the HS structure, and the heat transfer between the segments and energy equation per unit volume that describe the HS model are given by (16) and (17):

$$Q_{trans}(t) = kA\Delta T/x \tag{16}$$

$$\rho_d C_p \frac{\partial T}{\partial t} = -\left(\frac{\partial q_x}{\partial x} + \frac{\partial q_y}{\partial y} + \frac{\partial q_z}{\partial z}\right) + \dot{q} \tag{17}$$

where Q_{trans} is the heat energy transferred in unit time by segment, ΔT is the temperature gradient, x is the material thickness, ρ is the material density, Cp is the specific heat of the material, and q is the heat flux per volume.

The heat sink transfer to deep space can occur only through radiation, which is described by Equation (18):

$$Q_{rad} = \varepsilon\sigma A\Delta T^4 \tag{18}$$

where $Qrad$ is the radiated heat, and ε is the emissivity of the material.

For the numerical solution, the finite volume method was implemented in Visio OTK as part of MS Visio with the thermal solver Sinda. In the studied model, the alumina layer of the cold side of the TEG is replaced with an insulator with different thermal conductivity for studying the effect of the TEG on the HS efficiency. Through simulation, it was shown that for a k = 0.01 W/mK, the temperature of the PV reached 92.51 °C (instead of 50 °C in the case of the PV alone), which decreased its efficiency to 23.8% (instead of 26.7%). Due to this high temperature gradient through the TEG, its efficiency was 5.85%, which increased the overall efficiency of the HS to 29.65%. In this situation, the TEG increased the efficiency of the PV by 21.9%. However, using an insulator with a thermal conductivity larger than 0.1 W/mK could decrease the efficiency of the HS below the efficiency of the PV system, due to the fact that the heat sink works only through radiation transfer, without any convection transfer.

A novel HS system was proposed in [38] starting from the PV-TEG directly coupled structure by adding a TEC between the PV and TEG. The TEC has the role of cooling the PV, and the TEG has a role of a heat sink for the TEC and, based on the Seebeck effect, harvests the heat from the TEC. The system is used in high concentrated light. A MATLAB-Simulink model was developed for the triple-junction PV cell, which allowed observing the behavior of the cell and of each subcell at different concentration ratios (300–1000 suns). The model demonstrates the I–V and P–V characteristics and the temperature for the corresponding concentration ratios. For studying the PV-TEC-TEG HS, a finite element model was developed using MATLAB-Simulink and COMSOL Multiphysics. The model considers that the internal parameters of the TEC and TEG are similar. The paper compares the simulated results with the experimental results obtained from a real model composed of a $GaInP_2$/GaAs/Ge cell (manufactured by Shanghai Yim Machinery Equipment, China), a CP-12706 TEC ($40 \times 40 \times 3.92$ mm^3) connected through a copper bloc to the PV cell, a TEG1-31-2.8-1.2 TEG ($20 \times 20 \times 3.4$ mm^3) connected directly to the TEG and a copper heat sink. The temperature of the PV and the surfaces of the TEC and TEG were measured with the GM1312 thermometer (BENETECH Company, China) using K type thermocouples. Through this study, it was shown that due to TEC usage, the temperature of the PV decreased by ~46 and ~126 K at 300 and 1000 suns, respectively. The PV power increased due to the TEC cooling by ~3.8 and ~4.22% at 300 and 1000 suns, respectively. The power added by the TEG increased the overall system power by ~0.25% and ~0.5% at 300 and 1000 suns, respectively.

A numerical investigation into an indirectly coupled PV-TEG HS using heat pipes was carried out in [21]. The system was based on a boiling–condensing system based on heat pipes (Figure 4). The evaporator section of the heat pipes was intimately connected to the PV, extracting the PV heat, which through the condenser section was transferred to the hot side of the TEG. In order to increase the heat absorption from the sunlight, a black Tedlar-Polyester-Tellar (TPT) layer was added under the PV. Based on the partial differential equation model described in [21], numerically solved, it was shown that the efficiency of the proposed HS was better than that of a conventional PV panel. The efficiency difference decreased with the wind speed but increased with an ambient temperature and irradiance increase. The results in the paper show that the system is more efficient than the conventional PV panel only if the irradiance is larger than 200 W/m^2.

Kolahan et al. [39] evaluated the performance of two PVT and PVT-TEG HSs through numerical analysis. The partial differential equation models for both HSs were described and simulated based on a tridiagonal matrix algorithm using an implicit formulation, discretizing by a center-differencing scheme implemented in FORTRAN. The global electrical efficiency of the PVT-TEG HS was better than that of the PVT HS by 2.5–4%, while the overall energy efficiency presented an opposite behavior, being 1.67–1.83% smaller in the case of the PVT-TEG. Still, the global overall energy was larger by 2.17–3.13% in the case of the first one, and also, the payback period was smaller by 12%, increasing the income by 33% after 10 years. Gu et al. [19] propose a new mathematical model for the PV-TEG HS under concentrated sunlight based on thermal resistance theory. The model was solved based on the finite element method using the MATLAB software. It was found that reducing the thermal resistance of the heat sink used for cooling the TEG is a very important way of enhancing the HS efficiency.

The indirectly coupled HSs were studied in [40] by introducing a beam splitter (BS) (see Figure 5). The study was oriented to the design and optimization of a beam splitter in order to maximize the energy generation by the HS considering amorphous and multi-crystalline Si cells. The proposed model was numerically solved based on the Nelder–Mead simplex algorithm using the MATLAB software. Skjølstrup and Søndergaard showed that the efficiency of an HS with an optimized BS can be increased by 13.2 and 21.4% for the case of mSi and aSi, respectively, compared with a single PV cell. Yang et al. [41] propose an updated model for a BS used in PV-TEG HS. A detailed analysis was focused on the influence of the area ratio of the thermal collector of the TEG to the PV cell on the output and efficiency of the HS. The results show that the optimal area ratio is closely dependent on the light concentration. Yin et al. [42] propose a method for optimizing the BS for a PV-TEG HS from the optimal operating temperature and cutoff wavelength point of view. The results show that the optimal HS efficiency increases with the figure of merit of the used TEG, and the optimal cutoff wavelength decreases when increasing the ZT.

A numerical study that included a beam splitter was performed by Mohammadnia et al. [43]. The proposed HS has a concentrated photovoltaic (CPV)/Stirling engine/TEG structure, which is an indirectly coupled one. The light contractor is based on a parabolic mirror that contains the beam splitter in the focal point. The BS transmits the shorter wavelength to the CPV and reflects the longer wavelength to the Stirling/TEG assembly. The model equations are modeled using the Engineering Equation Solver (EES) software. The proposed system presents an optimal concentration ratio, which is 431.4 suns generating 38.34 kW of electrical power and having a 24.57% solar-to-electricity efficiency. The TEG contribution to the system generation is 0.97% of the electrical power, increasing the system cost by 0.32%. A similar study was presented by Mohammadnia et al. [44], but the BS had an opposite behavior, transmitting the longer wavelength to the Stirling/TEG structure and reflecting the shorter wavelength to the CPV. The same software package was used for numerical modeling. The results show an overall system efficiency of 21.8%, with 45.4 kW of electric power generation with 455 suns.

A three-diode numerical model of a PVT/TE HS was proposed and studied by Salari in [45] considering that the TEG was placed between the PV Tedlar layer and the copper absorber plate of the thermal collector. The study was oriented to comparing the PVT HS with the PVT/TE HS. The HS structure was a directly coupled one. The partial differential equations that model the proposed HS were solved based on the finite volume method. The results show that the electrical efficiency of the PVT/TE is higher than that of the PVT, while the thermal efficiency is lower. The effects of the irradiance, fluid mass flow rate, ambient temperature and inlet temperature variation were also studied, showing that the efficiencies of both HSs were dependent on these working factors. For example, in the case of an ambient temperature increase, the electrical efficiency of the PVT/TE increased, due to the TEG contribution, while the efficiency of the PVT decreased. The thermal efficiencies of both HSs were enhanced by the ambient temperature increase.

An indirectly coupled PV-TEG HS based on a flat heat pipe system under concentrated light was modeled in [46]. The COMSOL 5.4 Multiphysics software and three-diode finite element method were used for the proposed model simulation. A PV-only system and a directly coupled PV-TEG HS were used as references. By comparing the three systems, it was found that the efficiency was higher in the case of the PV-TEG with a flat heat pipe by 1.47 and 61.01% than that of the PV-TEG and PV-only systems, respectively.

4.2. Experimental Studies

This section is dedicated to the papers that are focused on experimental study, even those including the numerical approach.

Different instruments and apparatus are used for HS system characterization. The used instruments depend on the application scope:

A. Inside/outside characterization;
B. Long/short monitoring time;

C. Performance;
D. Cost.

A PV-TEC HS was proposed by Benghanem et al. in [7] in order to increase the PV's performance through its cooling using a TEC. The measurement system for HS characterization was composed of a Keithley 2420 source meter (Keithley Instruments Inc) used for I–V characteristic measurement, a CM11 Pyranometer (Kipp & Zonen Delft) used for radiation measurement, and a DMM 3695 (PeakTech) used for temperature measurement using K-type thermocouples. The results show that when using the TEC as a cooling system, the PV efficiency is increased by 0.19 to 1.3% per °C. The paper proposes using an additional PV panel for powering the TECs. The additional cost estimated in the paper through adding the TEC and secondary PV panel is only 6%, but this cost could be decreased for larger-scale PV systems.

The behavior of the directly coupled PV-TEG HS at a low solar concentration was studied by Mahmoudinezhad et al. in [47] and [48]. The studies were accomplished based on a solar simulator with xenon arc lamps. The solar concentration ratio was up to 39 suns. The HSs used were composed of a triple-junction InGaP/InGaAs/Ge solar cell (with an active area of 10 × 10 mm) and a Bi_2Te_3 TEG (with an area of 8.7 × 8.7 mm) connected to a water-cooled copper heat sink. The measurement system was developed around the NI cRIO 9074 platform, with dedicated modules for voltage, current and temperature measurements and the NI LabVIEW programming language used as controlling and data analysis software. The I–V–P characteristics were used as a characterization method. The scheme of the used experimental setup is presented in Figure 10. The same system was used in [31], where more details are offered regarding the uncertainties of the measurements obtained with the developed system. In [47], the HS's responses to different solar concentration levels were studied, experimentally but also numerically. For numerical simulation, the MATLAB software was used for solving the partial differential equation of the proposed HS model. The paper shows that the ratio between the maximum power generated by the TEG and that generated by the CPV increases once with the solar concentration. In [48], the transient response of the HS was investigated. A time-dependent pattern of the solar concentration level was applied to the HS, and its components' responses were monitored. The investigation was accomplished both experimentally and numerically. For numerical analysis, the COMSOL Multiphysics Modeling Software was used. The results illustrate that the CPV had a rapid response to the light variation, which was altered in time due to the temperature variation, while the TEG response was more gradual, almost following the temperature variation. This behavior of the HS components indicates that the TEG increases the stability of the generated power of the PV.

A simple and low-cost system was used in [49]. The characterization system was developed around the Arduino Uno R3 microcontroller-based board. The characterization system was developed for a directly coupled PV-TEG structure with a passive heat sink. The system used two DS18B20 digital sensors for the temperature measurements of the upper and lower sides of the TEG, and an INA219 current/voltage sensor that allowed measuring, simultaneously with the same chip, the current and the voltage generated by the studied system. The data read from sensors were stored on a SD memory card attached to the Arduino board. The HS was composed of a 170 × 110 mm PV panel, a SP1848-27145 TEG and a copper heat sink.

The influence of the cooling fluids and materials used on the heat sink attached to the cooled side of the TEG, in a directly coupled PV-TEG HS, was experimentally studied by Rajaee et al. [20]. Two scenarios were used for testing the HS. In the first scenario, fluids were used as a cooling system (pure water and 0.25, 0.5 and 1% Co_3O_4/water nanofluids), and in the second one, a layer of phase change material (PCM) (paraffin wax and paraffin wax with Al_2O_3 powder) was added to the 1% Co_3O_4/water nanofluid. The used components were: a crystalline silicone panel manufactured by EVERSUN SOLAR TECHNOLOGY with 300 × 155 × 17 mm dimensions; six-TEG model SP1848-27145, made by Shenzhen Yuzens Technologies Company, with 40 × 40 × 3.6 mm dimensions; and two aluminum sheets placed between the HS components and copper pipes for the fluid-based cooling system. As characterization instruments were used the following: two UT71C/S/E DMMs used for

current and voltage measurements, a TESTO-177-T4 data logger for temperature and data recording, and K-type thermocouples. There is no information mentioned about how the electrical power of the HS was determined using I–V characteristics or using a fixed load. The results show that at noon, the HS with 1% nanofluid increased the electrical power generated and the efficiency by 10.91 and 6.73%, in comparison with the HS with water, respectively. Adding the PCM layer further increased the overall efficiency of the system. In the case of the PCM with alumina powder, an increase in the electrical power of 4.52% compared to the 1% nanofluid case was obtained.

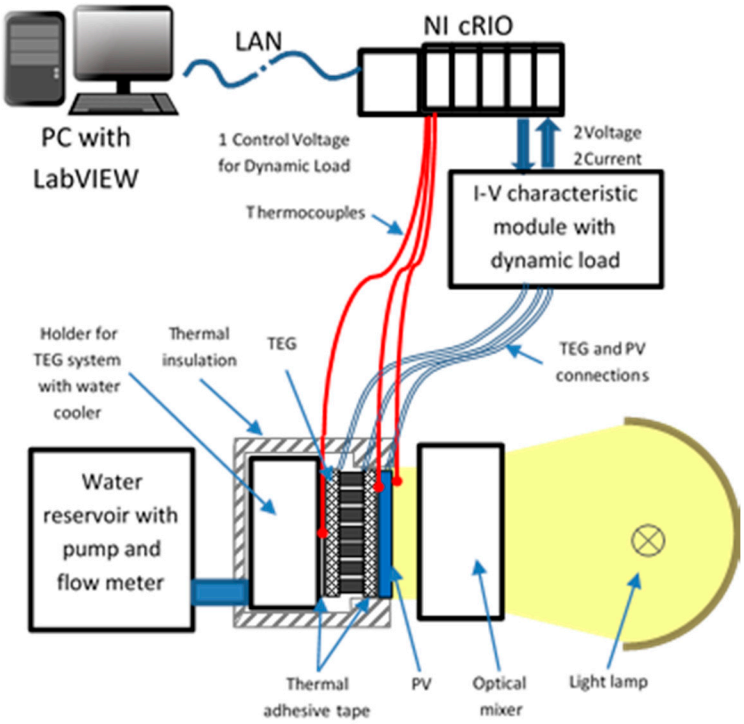

Figure 10. The experimental setup used for HS characterization under concentrated light [47].

In [50], the feasibility of harvesting the heat from PVs with TEGs was analyzed. The study considered using such HSs in a Hybrid Agrivoltaic Greenhouse System. The study was oriented to monitoring the PV temperatures (top, bottom and the air under the PV) in order to evaluate the potential thermal energy that could be harvested using TEGs. For temperature monitoring and distribution, a temperature data logger model SDL200 (EXTECH Instruments) with a K-type thermocouple and a Fluke thermal imager model Ti125 were used. Through calculus based on a developed mathematical model of 160 TEGs connected in series/parallel attached on the back of the PV module and on temperature measurements, it was shown that the maximum energy generated by the TEGs could reach the value of 119.18 W at a 56.1 °C temperature difference at noon. In the case of rain, the temperature of the PV decreases rapidly and the contribution of the TEGs is considerably reduced.

A directly coupled PV-TEG HS for natural light and based on the load requirement was designed by Shatar et al. [51] under a tropical climate. The block diagram of the proposed HS is shown in Figure 11. The HS consists of 4 × ADL100-12V PV panels (1200 × 540 × 30 mm), 12 × SP1848–27145 Bi_2Te_3 TEGs (40 × 40 × 3.4 mm), 3 × PGEL-100–12 Lead Acid batteries (12 V, 100 Ah) and a solar charger controller (30 A). The PV panels and the batteries were connected in parallel, and both, to the solar charger controller. The TEGs were connected in different configurations: all in series, two groups in parallel, each composed of six in series and three groups in parallel, and each composed of four in series. The solar charger controller was also used for the PV, battery and load parameters; ambient temperature measurements; and data logging (the power generated, state of charge and power absorbed, respectively). The V_{OC} of the TEGs and the PV temperature were measured using a NI

USB-6211 DAQ. K-type thermocouples were used as temperature sensors. An interesting result is described in the paper; namely, during the night, there was a temperature difference between the PV and the ambient temperature (the cold side of the TEG), which resulted in electrical generation during the entire night.

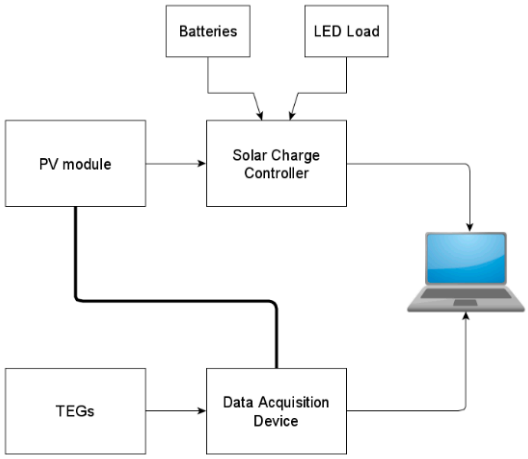

Figure 11. The setup of a PV-TEG with battery HS for indoor farming [51].

Piarah et al. [52] characterized a spectrum splitter for an indirectly coupled PV-TEG HS. They considered two spectrum splitters, the first with a hot mirror and the second with a cold mirror, and analyzed the right positioning of both the PV and TEG modules relative to the transmitted or reflected radiance. They found that the positioning of the PV and TEG in reflected and transmitted radiation in the case of using a spectrum splitter with a cold mirror offered better overall electrical power generation. The I–V and P–V characteristics were used as characterization methods. The current and voltage of both the PV and TEG modules were measured using six GW Instek GDM-8135 DMMs. A mini USB spectrometer with the Menges Spectragryph v.1.2. software for spectrum splitter transmittance and reflectance was used.

In [53], a study of using one or two BSs with different cutoff wavelengths for two and three types of PVs was performed. In this study, Si-based and InGaAs PVs were used for the first setup and GaAsP; Si-based and Ge PVs were used for the second setup. In the first setup, a BS with a cutoff wavelength of 950 nm was used, reflecting the shorter wavelength to the SI-based PV (IXOLAR KXOB 22-12X1) and transmitting the longer wavelength to the InGaAs PV (Hamamatsu Photonics G8370-02). The second setup included two BSs having a cutoff wavelength of 600 nm, reflecting the shorter wavelength to the GaAsP PV (Hamamatsu Photonics G1116) and transmitting the longer wavelength to the second BS, from the first setup (950 nm cutoff wavelength, with the Si-based (OSRAM BPW 34) and Ge (Thorlabs FDG03) PVs placed in the reflected and transmitted light, respectively). The study was carried out in artificial light (using a 2000 Abet Technologies solar simulator) and in natural solar light. The following instruments were used for characterization: a Keithley 2401 sourcemeter to measure the I–V characteristics of the PVs using a switching box that allows individually connecting, in series or in parallel, the investigated PVs; a pyranometer connected to a Keithley 181 nanovoltmeter for irradiance measurements; and a PT100 sensor connected to a Keithley 2001 electrometer for temperature measurements. Bruzzi et al. found that both systems have better efficiency compared to the Si-based PV alone. At best, the efficiency of the systems was doubled compared to that of the Si-based PV alone.

A new design for the HS was proposed in [54] with a PV-TEG-T structure like that in Figure 3. The motivations for using such a structure are based on the space occupied by all three HS components, increasing the electrical energy production and life time of the PV by decreasing its temperature with the TEG and solar thermal collector (STC). The paper analyzes two HS types; the first is based on

an mSi PV cell, a TEC1-12730 as the TEG and a solar thermal collector made from a flat copper block, while the second is based on four mSi or mSi PV cells connected in series, two TEGs of type TEC1-12730 connected in series and a solar thermal collector made from copper pipes. In the second case, the STC is larger than the PV-TEG structure and painted black to increase the thermal efficiency of the HS. The study was conducted under natural light conditions. For measuring the electrical and thermal performance of the HS components, the same system as that used in [47] and [48] was used. A SPN1 Delta T pyranometer and a flow meter for irradiance and water flow measurements were added to the characterization system. The environmental conditions were monitored with the help of a weather station, and the temperature distribution for the PV cells was analyzed with the help of a Testo 875i thermal imaging camera. By using the TEG and STC, the PV temperature decreased by 11 °C for an irradiance of 1000 W/m^2. The effect of the STC with a water flow that was active and stopped over the PV and TEG was significant, showing a reduction in the TEG and PV power generation by three times and 11%, respectively.

Popov et al. [55] used the virtual instrumentation for PVT hybrid characterization, also including uncertainty calculations. The characterization system was based on a LabJack UE9 DAQ and a self-developed extension board that offers 32 channels for temperature measurements using Pt100 sensors, 16 differential low-voltage channels for DC current, solar irradiance, thermocouple measurements, 10 voltage channels for AC voltage and current measurements, 8 counter channels for flow rate measurements and 1 wire interface that allows communication with up to 128 DS1820 temperature sensors. The irradiance was measured based on a Kipp & Zonen CMP6 pyranometer. For DC voltage measurements, the operational amplifier MCP609 was used as a signal conditioner, and an analog multiplexer HCF4051B was used for increasing the number of analog input channels. For current measurements, a shunt resistor with 0.1% accuracy was used.

Lashin et al. [56] proposed a new approach for a PV-TEG HS study. The proposed HS consisted of a Fresnel Lens, a CPV, a TEG and a heat sink thermal, connected with one another, the heat sink being immersed in flowing water. The study was accomplished in an indoor environment and consisted of replacing the FL and the CPV with five high-power resistors for emulating the heat generation by the CPV. Controlling the number of the active resistors and also the electrical power delivered to the resistors, through five power supplies, the number of solar cells and solar concentration levels were emulated (70, 100 and 130 suns). K-type thermocouples were used for temperature measurements of both TEG sides. The measurement of the current, voltage and temperatures was performed with DMMs, without offering any information about their performance. Based on this approach, the HS system could be studied through one of its components while the other was emulated.

An experimental and numerical investigation of a large-scale concentrated photovoltaic thermal HS with a TEG was conducted by Riahi et al. in [57]. In this paper, two HSs were compared, namely, CPVT and CPVT-TEG HS. The sunlight concentration was obtained using a parabolic trough concentrator fixed on a sun tracker. An mSi PV, two TEGs of type TEC1-12706 and an aluminum heat exchanger with circular multi-channels represented the components of the two HSs studied. The electrical and thermal characterization was based on a Keithley DAQ model 2700, K-type thermocouples and a variable resistor as the PV and TEG load. The numerical model was developed based on energy balance equations and implemented in the Engineering Equation Solver (EES) software. Comparing the results obtained for both the HSs used showed that the electrical efficiency of the CPVT-TEG was higher than that of the CVT by 7.46%, while the thermal efficiency showed an opposite behavior (47.53% for CPVT and 46.13% for CPVT-TEG).

An experimental study for an indirectly coupled HS like that in Figure 4 was performed by Shittu et al. in [22]. The heat of the PV panel was transferred to the TEG using a flat-plate micro-channel heat pipe (MCHP) through evaporation and condensation processes. The TEG was attached on the hot side to the condenser region and on the cold side to a heat sink, which consisted of an aluminum water-cooling block (which can act as a thermal collector, increasing the water temperature of the water in the water tank used as a cooling system). The electrical performance of the PV module was

measured based on an ISM 490 solar analyzer manufactured by RS Pro, while that for the TEG was measured based on Aneng AN8009 and Neoteck DMMs and an Earlywish Variable decade resistor. The temperatures were measured based on K-type thermocouples and a Hioki data logger. The used components were an unglazed crystalline silicon PV and a TEG of type GM250-127-14-16. The analysis of the HS showed that the efficiencies of the PV in the HS and alone were 12.19 and 11.94%, while its working temperatures were 61.9 and 67.9 °C after 1 hour. The thermal efficiency of the system reached the maximum value of 69.53% under the irradiance of 500 W/m^2.

A numerical and experimental study was conducted by Zhou et al. in [58] on an HS that used a perovskite solar cell (PSC) as the PV component. The numerical simulation of the proposed model was performed using the MATLAB software. The experimental setup for the PSC-TEG HS consisted of a PSC with a composition of $CH_3NH_3Pb(I_{0.95}Br_{0.05})$, a TEG of model XH-F241A1126 (Xinghe Electronic Technology Co.), a Keithley source meter of model 2400 for J–V characteristic measurements, an Oriel solar simulator of model 91192 and a calibrated silicon standard solar cell for irradiance measurements, a water-cooled heat sink, and K-type thermocouples of model SMPW-TT-K-30-SLE (OMEGA). The results show that the PSC alone had an efficiency of 18.2%, while the HS could achieve an efficiency of 23%, due to the energy cogeneration of the TEG.

An experimental study of a PV-TEG-MCHP HS was conducted by Li et al. in [59]. The HS performance was compared with that of a PV-only system. The indirectly coupled structure of the HS used was like the one shown in Figure 4 and consisted of a crystalline Si cell, a Bi_2Te_3-based TEG and a flat aluminum plate heat pipe as an MCHP. The testing system consisted of an RS Components solar module analyzer of model ISM490, two Neoteck pocket DMMs, an Agilent DAQ of model 34970A, five copper–constantan thermocouples, a Jinzhou Pyranometer of model TBQ-2 and a Jinzhou ambient monitor of model JZH-1. The TEG electrical parameters were determined using the Neoteck DMMs and a variable resistance load. The results obtained for different irradiance, wind speed and ambient temperature conditions show that in all the considered cases, the PV-TEG-MCHP produced more electrical energy compared to the PV only, even if the PV temperature in the HS case was higher. The maximum electrical efficiency of the HS was 14.3% compared to that of the PV only, which was 13.6%.

4.3. Independent Component Characterization Studies

Different methods and instruments for PV and TEC/TEG characterization have been developed and presented in the specialist literature. This section presents some of the most used systems for individual HS component characterization.

4.3.1. TEG Characterization

In the case of the thermoelectric module used as a TEC, considering the characteristic parameter constants during the working conditions introduces errors. In [60–62], Ahiska et al. proposed a new method and designed a system called the Thermoelectric Performance Analysis System (TEPAS) that allows the TE characteristic parameters' determination. It is presented how the experimental parameters I_{max}, V_{max} and E_{max} and output parameters P, Z, K, R and τ (the time constant of the TE module) could be determined under the working conditions. A comparison with the classical methods was performed, showing that there are considerable differences. In the case of the coefficient of performance (COP), the errors varied from 3.3 to 19.9% [61], while for τ, the error varied from 3 to 16% [62] for the proposed method and the classical ones.

A methodology for TEG characterization is presented in [63]. Carmo et al. studied a commercial TEG of type TEC1-12707 at different temperature gradients created with the help of a controlled hot-plate and a cooling fan. The hot-plate and the cooling fun were in contact with the hot and cold sides of the TEG, respectively, through two copper plates that assured a better temperature contact and uniformity. The temperatures of both TEG sides were measured using two thermistors in a bridge circuit. For controlling the temperature differences, a PC with LabVIEW and an NI USB-6009 DAQ board were used. The control was ensured through two closed-loop controlling

systems that ensured the temperature differences even if the TEG was under an open circuit or load working conditions. The current and voltage generated by the TEG for different values of the applied load (manually adjusted) were measured using the Agilent 34410A multimeter. The TEG characteristic parameters obtained were the internal resistance R_{int} = 3.88 ± 0.13Ω and the open circuit voltage V_{OC} = 53.17 × ΔT (mV). The considered range of the ΔT was 8–75 °C, with a hot side temperature range of 47–126 °C. The behavior of the TEG in a low temperature range of 100–300K was studied by Karabetoglu et al. in [64] using a controlled electrical heater for the hot side and a cooler based on liquefied nitrogen for the cold side. The temperature gradient was maintained at 20K. The uncertainties of the used sensors were ±0.04, ±1, ±0.5 and ±3% for the temperature, heat flux, current and voltage measurements, but the used equipment and sensor types were not mentioned.

A system for TEG characterization based on programmable logic controller (PLC) was developed by Ahiska et al. in [65]. An S7-200 CPU224XP PLC with an EM 231 extension module was used for data acquisition. The MCR-VDC-UI-B-DC and WAS2 CMA 5/10A transducers connected to the EM231 module were used for voltage and current measurements, respectively. Two ARF-4 turbine flow meters were used for measuring the flow of the hot and cold fluids. The flow meters were connected to two high-speed counters of the PLC, obtaining a ~1% measurement accuracy. The voltage, current and temperature measurements were calibrated using a Fluke 725 Multifunction Process Calibrator device. For PLC and PC application development, the MicroWin program and WinTr SCADA software were used, respectively. The relative errors reported in the paper compared with the datasheet for the tested Altec-GM-1 TEGs were around 4 and 3% for the maximum power and efficiency.

Liu et al. [66] designed and tested a 500 W low-temperature thermoelectric generator. Their approach was to test different modules before designing the 500 W module. The chosen module was a Be_2Te_3-based TEG with a 40 × 40 mm size and 127 couples. The global efficiency concept introduced in this paper is determined as the ratio of electrical energy generated by the TEG to the total thermal energy of the used liquid for heating the TEG's hot side. The value of the global efficiency obtained for one module was about 10%, while for the 500 W module (built from 96 modules), the global efficiency was about 9%. For the last, the electrical power generated at 80 °C temperature differences (100 °C for the hot side and 20 °C for the cold side) was 160 W. In order to obtain a 500 W power output, a 200 °C temperature difference should be created.

A solar thermoelectric generator was designed and studied by Özdemir et al. [67]. The system was based on a solar thermal collector composed of a reflector and a solar collector tube, with a heat pipe connected to a TEG on its hot side and an aluminum heat sink connected to the cold side of the TEG. The heat sink was placed into a wind chimney for cooling down and thus cooling the cold side of the TEGs. The results show that the power generated by the TEG reached the maximum value at 1:30 p.m., which does not correspond to the time of the maximum irradiance. This is due to the fact that the time period when the maximum temperature difference was reached did not overlap with the time of the maximum irradiance. The maximum power generated by the TEG was 0.83 W, with a maximum efficiency of 0.46% at a 110.7 °C temperature difference. The instruments used for the measurements were a data logger ORDEL UDL100 with an accuracy of 0.2%, K-type thermocouples connected to the data logger, an HD 2303.0-Delta OHM anemometer used for air flow measurements through a chimney, a MASTECH MS8221 Multimeter and a DeltaOhm LP PYRA 02 pyranometer for TEG V_{OC} and irradiance measurements, respectively. A Bi_2Te_3-based TEG1-12611-6.0-type module was used, characterized by a 56 × 56 × 4 mm size and 126 couples. The maximum power was calculated based on the V_{OC} and an internal resistance considered fixed at 1.2 Ω.

A microcontroller-based system for TEG characterization was developed by Izidoro et al. [29,68]. The system allowed simultaneously characterizing up to three TEGs. The system was based on two 40 MHz clock PIC18F452 microcontrollers that were used for data acquisition and output control. The TEG sides' temperatures were measured using K-type thermocouples using the MAX31855 chip. Voltage divisors and ACS712-5 chips for measurements of the generated voltage and current, respectively, were used. For heating the TEG hot side, a 1500 W AC-powered electrical heating

resistor with PWM control was used, while for cooling the TEG cold side, an aluminum heat sink with a DC-powered fan with PWM control was used. The errors of the system without calibration were 12, 4 and 5% for the temperature, voltage and current, respectively. After calibration, the errors decreased to the values of 5, ±1.5 and 2%. The software used for system control and data processing was Borland Delphi 7.0®. For measuring the I–V and P–V characteristics of the TEGs, a power resistor set was used as the electrical load.

A TEG model was developed and simulated using the TRNSYS and Fortran software, and experimentally validated in [69]. The nonlinear differential equations were solved in Fortran based on finite differences and Newton–Raphson methods. The experimental study was based on an electrical heat source and an active water-cooled heat sink. The temperatures of the TEG sides placed between the heater and heat sink were measured using K-type thermocouples. A NI cRIO platform with an I/O module was used for temperature, current and voltage measurements. The comparison of the numerical and experimental results for the temperature and electrical output power showed normalized root-mean-square errors of 3.53 and 2.33%, respectively.

A numerical and experimental TEG characterization under a low temperature difference was performed by Al Musleh et al. in [70] with applicability in powering the sensors and IoT devices for building applications. The considered range of the temperature difference was 10 °C for this study. For TEG characterization, a testing system was built and consisted of two copper water blocks used as a heater and cooler for the TEG sides. The hot and cold water cycles were controlled with a PID controlled heat exchanger unit of type WL 110 from G.U.N.T. Gerätebau GmbH, and the temperatures of the inlet and outlet water for the two water blocks were measured using PT100 RTD sensors. The water flow rate was determined with a paddle-wheel flow meter of type Bürkert 783724Y. The electrical parameters of the TEG were determined with an I–V tracer, the RO2—I–V TRACER from Thermoelectric Conversion Systems Ltd. The numerical analysis was performed using the COMSOL Multiphysics software. The comparison of the experimental and simulation results showed a good match, with a root-mean-square deviation under 5%.

4.3.2. PV Characterization

In this section are discussed and presented the systems and methods used for the PV I–V characteristic measurements. According to Zhu and Xiao [71], there are five methods used in the literature for the I–V characteristic measurements of PV modules or arrays. In order to measure the I–V characteristics, a variable load should be applied to the PV such that the zero to open circuit voltage range is covered. Such a variable load can be designed using a variable resistor, a capacitor electronic load, a four-quadrant power supply (FQPS) or a DC–DC convertor. Short descriptions of the first four methods are presented in [72], where are also presented some analytical methods that allow determining the important PV parameters from the I–V characteristics.

Resistor-Based Method (RBM)

Amiry et al. [73] designed a low-cost I–V tracer for PV characterization under real working conditions. The I–V tracer was developed around the Arduino Mega board, which was connected to a PC, being based on a set of resistors that are activated through an equal number of N-MOSFET (IRF540N). The used resistors permitted measuring the entire I–V curve, but the values of the used resistors were not mentioned. For each measured point of the PV I–V characteristics, a 1 ms time interval was necessary. The current was measured using an INA 219 DC current and voltage sensor. The resolutions of the current and voltage sensor were 1 mA (accuracy of 1%) and 4.89 mV, respectively. The temperature was measured using K-type thermocouples using the MAX6675 chip. The Solarimeter—SL200 device was used for irradiance measurements.

Transistor-Based Electronic Load Method (TBM)

A simple circuit that works as a dynamic load for the I–V characteristics of a PV measurement is described in [74]. The circuit is based on the MOSFET technique in the configuration of a slope generator using the capacitance C between the drain and gate terminals of the IRF540N N-MOSFET transistor. A square-wave generator based on a NE555 chip is created and is connected to the N-MOSFET slope generator. The C has the goal of maintaining the MOSFET in the amplification region during its charging–discharging process at each commutation of the square-wave generator. A complete system for I–V characteristic measurement also based on the MOSFET technique is described by Taciuc in [75]. The slope generator is based on a timer, and an operational amplifier is connected to IRF 2907 N-MOSFET transistors. A 12-bit ADC device with 40 analog input channels and a ±0.1% sampling accuracy was used for measurements. A resistive voltage divisor, a Hall effect-based current sensor ACS713 (Allegro MicroSystems), a pyranometer SMP11 (Kipp & Zonen), an anemometer Adolf Thies GmbH & Co.KG, and NTC thermistors NTCM-HP-10K-1% (SR Passives) were used for voltage, current, irradiance, wind and temperature measurements, respectively. A more complex dynamic load for the I–V tracer based on TBM is presented in [76]. The I–V characteristics are measured in a double-sweep way. The first step starts from a V_{OC} point and moves to I_{SC} points in equal steps using a OpAmp voltage feedback loop (equidistant voltage steps) for transistor gate control, and then, the reverse movement is performed by using a OpAmp current feedback loop (equidistant current steps).

A plug-and-play I–V tracer based on TBM for PV characterization under real working conditions was implemented and presented in [77]. Sarikh et al. developed the I–V tracer around the Raspberry Pi single-board computer. They used an IRFP250 MOSFET transistor as the electronic load. For measuring the current and voltage, the AC712 Hall effect sensor and a voltage resistor divider were used. For the digitization of the sensor output, the I2C ADS1115 ADC was used. A shunted solar cell and a Pt-1000 RTD were used as sensors for irradiance and temperature measurements, respectively. For controlling the transistor, a PWM signal was generated by the RPi board and was applied to the transistor gate through a low-pass filter (LPF). The goal of the LPF is to convert the PWM signal into an analog voltage that controls the MOSFET gate-source.

Capacitor-Based Method (CBM)

Cáceres et al. present in [78] a low-cost characterization system for PVs based on an I–V curve tracer. The entire cost of the hardware and software is estimated to be lower than EUR 200. The system is based on the TivaC Series LaunchPad embedded system, which offers two independent 12-bit ADC 1 MS/s sampling rate and 48 GPIO lines. The capacitance method was used for PV I–V characteristic measurements. As signal conditioning, the AD620BNZ instrumentation amplifier from Analog Devices was used for current, temperature and irradiance (amplifier) and voltage (attenuator) measurements. For the current measurement, a shunt resistor of class 0.5 was used. The irradiance measurement was based on a pSi PV shunted with a resistor of class 0.5, and for temperature measurements, a PT100 resistor and an open-circuit pSi PV were used. The software application for system control, data analyses and result presentation was developed in NI LabVIEW 2019. Based on the calibration and certification of the system through certified laboratories, the obtained statistical error for the I–V characteristic measurements was lower than 1.6%. Still, the I–V tracer developed by Erkaya et al. [79] is based on the capacitor method. In this case, the capacitor is not pre-polarized, so the I–V characteristics do not reach the I_{SC} point. The tracer allows measuring the irradiance based on four small mSI cells connected in parallel and shunted with a 0.25 Ω resistor. The PV temperature is measured using a K-type thermocouple. The I–V tracer is designed for the characterization of PV arrays with a V_{OC} up to 600 V and I_{SC} up to 30 A.

The capacitor method with pre-polarization is presented and was implemented at the PV cell level by Cotfas [80], as a module for the RELab system. The modularity of the system allows studying the PVs, wind turbines and solar thermal collectors. The implemented schemata of the pre-polarized capacitor method is shown in Figure 12. In this manner, the entire I–C characteristic is obtained. Due to the

pre-polarization when the pre-charged capacitor is connected to the PV, it is discharged through the PV, and therefore, the I_{SC} point is reached. For data acquisition, the NI ELVIS II, NI myDAQ or NI myRIO devices were used. The performance of the developed I–V module was studied through comparison with the AUTOLAB PGSTAT 30 system [81]. Based on the same concept, a four-independent-channel dynamic load was designed for PV cells and panel characterization developed around the NI cRIO platform [31,47,48,82].

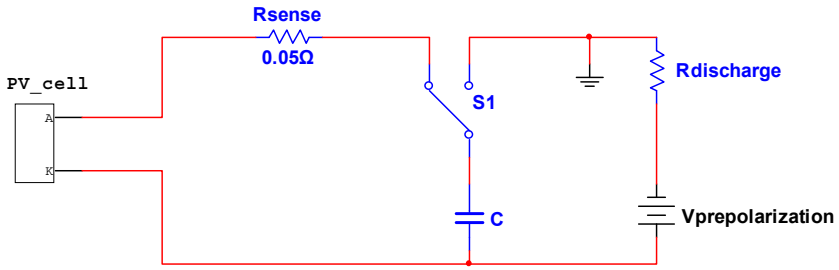

Figure 12. Pre-polarized capacitor implementation [81].

For PV array characterization, Chen et al. [83] designed a capacitor-based I–V tracer based on an embedded system. The system designed consists of capacitors, two IGBT transistors, an insulated solid-state relay (SSR) and a TMS320F28335 digital signal processor (DSP) connected to an LCD. One transistor has the goal of connecting the capacitors to the PVs for I–V characteristic measurements. The second transistor connected between the PV terminals allows measuring the I_{SC} (when it is switched on). With both transistors switched off, the V_{OC} can be measured. For capacitor discharging, the SSR is used, connecting the capacitor bank to a resistor bank. The LTS 15-NP and LV 25-P Hall effect sensors were used for current and voltage measurements. For control, data acquisition and processing, the DSP processor was used. In order to determine the important parameters of the PV, a metaheuristic hybrid algorithm based on an artificial bee colony and Nelder–Mead simplex algorithms was used.

The majority of the I–V tracer was supposed to disconnect the PV module from the PV string in order to measure the I–V characteristic. Ortega et al. [84] propose a new I–V tracer design based on CBM. Two very small capacitors in the range of microfarads are used for measuring the I–V characteristics in three steps, without using power electronics components. During the three steps, the operating point of the PV module is modified for a very small time interval, less than 5 ms, and with ±0.3 A and 5 V. Due to this short time interval and small current and voltage range variation, the PV module should not be disconnected from the string being tested in situ. The obtained accuracies for the I–V characteristic measurements are between 1 and 10%. For the maximum power point and short circuit current regions, the accuracies are less than 3%.

A portable I–V tracer for high voltage was developed and presented by García-Valverde et al. in [85]. The tracer was designed for organic photovoltaic modules with a V_{OC} larger than 5 kV and was based on CBM. One of the issues in the design of such an I–V tracer is the relay that should be used for such a high voltage. In this case, the GR5MTA relay triggered with a MOSFET transistor, together with an RC network as a snubber circuit, was used. The TM4C123G microcontroller, as a main control and measurement part, was used together with the TS912BIDT OpAmps as a signal conditioner for current and voltage measurement. A shunt resistor and a voltage divider for the current and voltage measurements were used, respectively. The sensors for the irradiance, temperature and humidity measurements were connected to an ArduinoMega2560R3 board. The data from the two microcontrollers were sent to a PC with the LabVIEW software application, through Bluetooth (main microcontroller) and USB (Arduino) connections. The low-power electronics were powered by a 12 V lead-acid battery.

The IoT Applied in PV Systems

Information technologies are more and more present in all fields of activities. IT became a strong part of the renewable energy domain, and the new concept of the Internet of Things—IoT—is now applied in PV system characterization and monitoring, too. Shapsough et al. [86] propose a monitoring architecture based on the IoT concept dedicated for PV systems. The architecture is structured with five layers: a perception layer—hardware for data acquisition and processing (edge computing); network layer—the wireless technologies used for connecting the measuring hardware with other parts of the system through the Internet; middleware layer—technologies dedicated for data storage, processing (even using AI and cloud computing) and message transfer; application layer—dedicated for user interfaces; and business layer—technologies and tools for interconnection with other services. The proof of concept of monitoring two PV panels (one clean and one covered with dust) for a period of two months was implemented. The I–V tracer is based on CBM, using two capacitors of 51 mF connected in parallel and three digital relays for connecting the capacitor to the PV and to the discharging resistor. The system was developed around a Raspberry Pi, which controls the relays, and communicates with the temperature and irradiance sensors and Yocotwatt wattmeter used for the current, voltage and power measurements with a sampling rate of 100 Hz. Using a WiFi network, the data are sent by the Raspberry Pi to the main server.

An IoT system dedicated for a decentralized PV plant was proposed by Pereira et al. in [87]. The IoT system allows monitoring the climate and PV parameters through an Analog/Digital Converter Embedded System (ADCES) based on the SanUSB microcontroller. The ADCES is serially connected to a Raspberry Pi platform. The sensors used for parameter monitoring are ACS712—5A, a resistive voltage divider, LM35, a pyranometer LP02, and DHT11 for the current, voltage, PV temperature, irradiance and ambient temperature and humidity, respectively. All the information saved on the cloud server are saved and visualized through a self-developed Web Monitor using PHP, Apache and MySQL. Another version of the developed monitoring system based on IoT is introduced in [88]. In this version, only the working condition parameters such as the PV temperature, irradiance, ambient temperature and humidity and wind speed are considered. The system is based on the ESP 32 Cloud on Chip module for PV temperature and irradiance measurements and ESP 8266 for wind speed and ambient temperature and humidity. Using WiFi connections, the data acquired by the two microcontrollers are sent to the Cloud server. Variants of PV monitoring systems based on IoT have been implemented and discussed by a large number of papers. Some of them are based on the Arduino platform along with different sensors and network connection solutions. Such systems based on Arduino Uno were analyzed and implemented in [89] using a SIM 900 GSM module, in [90] using a nanorouter with 3G capabilities, in [91] using a Wi-Fi ESP8266 module, and in [92] using an Arduino server architecture and a router for the network connection. There are solutions based on the Arduino Mega or RPi platform [93–97], which use in-built or different shields for network communication.

5. Discussion and Conclusions

The precise characterization of HS components is essential in research or for industrial applications. According to Ziolkowski et al. [98], through a round-robin campaign, it was noticed that the TEG properties are obtained with a 20% deviation. Therefore, Ziolkowski et al. propose a generic procedure for TEG characterization. Based on this procedure, it was found that the uncertainty of the heat flow determination for TEG characterization is between 0.2 and 0.75% if the Guarded Hot Plate-based absolute method is used. Based on the same idea, Carducci et al. [99] improved the unified method for TEM characterization through developing a novel measurement system, by replacing the temperature measurements using thermocouples with thermistors and their calibration, and also by reducing the number of used components. They showed, by comparing the results obtained through this new method with the ones based on thermocouples described in [100], that the uncertainty in the determination of the temperature-dependent parameters of the TEM decreased significantly. Thus, the uncertainty was reduced from 1.4 to 0.027 °C for temperature difference measurements. In the case

of a temperature difference of 3 °C, the Seebeck coefficient and figure-of-merit uncertainties decreased from 0.431 to 0.0037 V/K and from 160 to 0.58%, respectively.

In the case of PV, Popov et al. [55] introduce a methodology for in situ uncertainty determination for a PVT HS that allows reducing the test times by making the appropriate decisions during the tests. Such methods could be applied to PV and TEG characterization as components of an HS.

Table 1 summarizes the instruments used for an HS and its components' characterization. The electrical characterization of the HS components is performed using an I–V tracer or variable resistors using a sourcemeter, electronic loads or resistor blocks (the latter mostly for TEG). For a simple and low-cost solution, the characterization systems are based on Arduino or Raspberry Pi boards together with analog or digital sensors. The K-type thermocouples are the most used sensors for temperature measurements. Natural light is the most used test condition, but solar simulators are also used. In the case of characterization systems based on PCs, the LabVIEW software is mostly used.

As one can see from the Characteristics columns, information about the accuracies and uncertainties of the instruments and measurements is not always offered in the literature. Furthermore, the information offered differs from paper to paper. In some papers, only the accuracies are offered, without information about the uncertainties, or only the standard deviations or the experimental root mean square errors (RMSE) are provided. There are papers that do not offer information either about the measurement performance or about the used equipment, showing only the results. On the other hand, there are papers that indicate the exact model of the equipment used, and based on its datasheet provided by the manufacturer, the measurement accuracies or uncertainties can be determined, which can compensate for the lack of information about the measurement performance. From the Irradiance column, one can notice that there are many papers that omit information about the equipment used and/or its performance for irradiance measurements. As a new trend, IoT technologies are used for monitoring and characterizing PV systems or HSs, mostly for remote or large-scale platforms.

The Application scope column synthetizes the applicability of the reviewed instruments for HS or its components' characterization. There are instruments with high costs but with high performance such as source-meters, cRIO platforms and dedicated DMMs or systems based on microcontrollers or single-board computers that are low cost but show good PC or network connectivity, useful for remote monitoring, even if the performance is at a low or average level.

In Table 2, the software applications that are used for an HS and its components' simulations are presented. The most used software is MATLAB, which can be combined or not with Simulink. COMSOL Multiphysics is also one of the most used pieces of software for modeling and simulation. According to [32], these software packages are classified as open-architecture research tools. The equations of the proposed models are solved in the mentioned software based on finite element or finite volume methods, in the majority of cases.

The most studied type of HS structure in the literature is the directly coupled one, but complex structures that involve beam splitters and Sterling engines, such as in [43] and [44], have begun to be investigated in order to increase the overall efficiency of the HS.

The PV-TEG HS increases the electrical efficiency of the PV through the cogeneration contribution of the TEG, but also decreases the PV temperature. Working at low temperatures, the PV's efficiency and its life time are increased [54]. When comparing the PV, PVT and PVT-TEG HSs, one can notice that from the electrical point of view, the PVT-TEG has a better efficiency, while from the thermal energy cogeneration point of view, the PVT is better [45].

Analyzing the literature, one can notice that there are studies based only on experiments or only on numerical simulations, but there are also studies based on both. The remark of Sark [34], that in the real case, the contribution of the TEG to the overall HS efficiency could be smaller due to the approximations that are made in the numerical model, strengthens the idea that a study based on both approaches could offer more reliable results. In [38], the results obtained through both approaches are in good agreement, but comparing the electric potential of the TEG without the PV installed, at least a 7.5% difference is obtained. In the case of the PV and thermal collector outlet temperatures, average

errors of 1.6 and 1.3% were obtained in [25] based on experimental results from the literature. The same approach of comparing the numerical results with experimental ones taken from the literature was adopted in [30], where average errors of 7.4 and 8.3% for the power generated by the PV and TEG components were reported. The efficiency errors for the PV and TEG obtained in [47] were in the ranges of 5.6–9.9% and 6.25–16%, respectively, when the concentration ratio varied between 8 and 37. The obtained differences between the numerical and experimental approaches show that the approximations performed in the developed models could have an impact on the result quality, and the model validation should be conducted experimentally. Therefore, combining the two approaches represents a better way for obtaining reliable results.

Future Work on PV-TEG HS Development

Based on the results of recent papers considered in this review, some further research directions could be addressed:

- Developing new procedures and methodologies for HS system characterization to improve the quality of the measurements and decrease the measurement uncertainties.
- Improving the models of the HS components considering 3D approaches (even if there are already papers published that cover this field, they are only a few) for the better prediction of HS behavior.
- Developing dedicated instruments for PV-TEG HS characterization (at the component level or as a whole).
- Developing new and more complex HS structures by combining different energy harvesting components such as PVs, TEGs, PCM materials, Sterling engines and solar thermal collectors in order to increase the efficiency of the hybrid systems.
- Enlarging the scale of the studied PV-TEG HS at the farm level for a better understanding of the performance of the integrated system, the life cycle and the feasibility of the HS.
- Introducing distributed characterization systems based on modern IT concepts such as the IoT and cloud computing for large-scale systems.

Table 1. Used instruments.

Reference	Platform and Method		Current		Voltage		Temperature		Temp. Sensors		Irradiance		Testing Conditions/ Comments	Application Scope [4]
	Device	Characteristics	Device	Ch. [1]	Device	Ch. [1]	Device	Ch. [1]	Device	Ch. [1]	Device	Ch. [1]		
Hybrid system														
Benghanem et al. in [7]	PC	ReRa Tracer Software	Keithley 2420	-	Keithley 2420	-	PeakTech DMM 3695	-	K-type thermocouples	-	Kipp & Zonen CM11 Pyranometer	-	Natural light	A: Outside; B: Short; C: High; D. High.
Rajaee et al. [20]	-	-	DMM UT71C	MA[2] = ±(0.8% + 1) MSD[3] = 0.051	DMM UT71C	MA [2] = ±(0.6% + 1) MSD[3] = 0.046	TESTO -177-T4	MA [2] = ±0.5 MSD [3] = 0.14	K-type thermocouples	MA[2] = ±1 MSD[3] = 0.288	-	-	Natural light	A: Outside; B: Short; C: Average/High; D: Average
Mahmoudinezhad et al. [31,47,48]	NI cRIO 9074	LabVIEW	NI 9227 module	Resolution, 24 bits; Range, 5A_{RMS} Relative uncertainty, 0.26%	NI 9215 module	Resolution, 16 bits; Range, ±10 V Relative uncertainty, 2.34%	NI 9211, NI 9213 modules	Resolution, 24 bits; Range, ±80 mV/ ±78.125 mV Relative uncertainty, 0.09 and 0.03%	K-type thermocouples	-	Thermogauge sensor	-	Xenon lamps	A: Outside/ Inside; B: Long; C: High; D: Average/ High.
Indrasari et al. [49]	Arduino Uno R3	-	INA219	-	INA219	-	-	-	DS18B20	-	-	-	Natural light	A: Outside; B: Short; C: Low; D: Low.
Shatar et al. [51]	PC		Solar charger controller and NI NI USB-6211 DAQ	-	Solar charger controller and NI NI USB-6211 DAQ		Solar charger controller and NI NI USB-6211 DAQ		K-type thermocouple	-	-	-	Natural light	A: Outside; B: Long; C: Average; D: Average.
Piarah et al. [52]	-		DMM GW Instek GDM-8135	0.414 µA	DMM GW Instek GDM-8135	Power, 0.818 × 10^{-3} µW	-		-	-	Mini USB spectrometer	-	Halogen bulb and Fresnel lens	A: Inside; B: Short; C: Average/ High; D: High.
Bruzzi et al. [53]	PC	MATLAB	Keithley 2401 source meter	±10 µA	Keithley 2401 source meter	±1 mV	Keithley 2001	-	PT100	-	Pyranometer—Keithley 181 nanovoltmeter	±10 W/m^2	2000 Abet Technologies solar simulator and natural light	A: Inside/ Outside; B: Long; C: High; D: High.
Popov et al. [55]	PC	LabVIEW	LabJack UE9/MCP609 OpAmp/HCF4051B and 0.1% resistor	-	LabJack UE9/ MCP609,OpAmp/ HCF4051B		LabJack UE9/MCP609 OpAmp/HCF4051B or 1 wire interface	-	PT100/ DS1820	-	Kipp & Zonen CMP6 pyranometer	-	Natural light	A: Outside; B: Long; C: Average/ High; D: Average/ High.
Shittu et al. [22]			PV RS Pro ISM 490 TEG Aneng AN8009 DMM Earlywish Variable decade resistor	Accuracy ±1% ±0.5% ±1%	PV RS Pro ISM 490 TEG Neoteck Pocket DMM Earlywish Variable decade resistor	Accuracy, ±1% ±0.5% ±1%	Hioki Memory HiLogger LR8400	-	K-type thermocouple	Accuracy, ±0.5%	Hukseflux Pyranometer SR20-D2	Accuracy, ±1.2%	Atlas Solar simulator Solar constant MHG 4000/2500	A: Inside; B: Short; C: High; D: High.

Table 1. *Cont.*

Reference	Platform and Method		Current		Voltage		Temperature		Temp. Sensors		Irradiance		Testing Conditions/ Comments	Application Scope [4]
	Device	Characteristics	Device	Ch. [1]	Device	Ch. [1]	Device	Ch. [1]	Device	Ch. [1]	Device	Ch. [1]		
Hybrid system														
Riahi et al. [57]	PC	LabVIEW	Keithley DAQ 2700	-	Keithley DAQ 2700	-	Keithley DAQ 2700	-	K-type thermocouples	-	-	-	Natural light	A: Outside; B: Short/ Average; C: High; D: Average/ High.
Zhou et al. [58]	-	-	Keithley 2400 source meter	-	Keithley 2400 source meter	-	-	-	K-type thermocouple model SMPW-TT-K-30-SLE (OMEGA)	-	Calibrated silicon standard solar cell	-	Oriel solar simulator model 91192	A: Inside; B: Short/ Average; C: High; D: High.
Li et al. [59]	PC	-	PV RS Components Ltd.—ISM490 TEG Neoteck DMM	Accuracy, ±1% Experimental RME, ±1%	PV RS Components Ltd.—ISM490 TEG Neoteck DMM	Accuracy, ±1% Experimental RME, ±1%	Agilent DAQ 34970A	-	Copper–constantan thermocouples (homemade)	Accuracy, ±0.5 K Experimental RME, 0.33%	Jinzhou Pyranometer-TBQ-2	Accuracy, 2% Experimental RME, 2%	Natural light	A: Outside; B: Short; C: High; D: Average/ High.
PV Component Alone														
Amiry et al. [73]	Arduino Mega	Method: I–V with RBM	INA 219	Resolution, 1 mA Accuracy, 1%	INA 219	Resolution, 4.89 mV	MAX6675	Resolution, 0.25 °C	K-type thermocouple	-	Solarimeter —SL200	-	Natural light	A: Inside/ Outside; B: Short/ Average; C: Low; D: Low.
Taciuc [75]	12-bit ADC with 40 AI	Method: I–V with TBM	ADC and Allegro MicroSystems Hall effect-based current sensor ACS713	-	ADC and resistive voltage divisor	-	ADC	-	NTC thermistors NTCM-HP-10K-1% anemometer Adolf Thies GmbH & Co.KG	-	Kipp & Zonen SMP11 Pyranometer	-	Natural light	A: Inside/ Outside; B: Long; C: Low/ Average; D: Average/ High.
Cáceres et al. [78]	PC and TivaC Series LaunchPad	LabVIEW 12-bit ADC 1 MS/s sampling rate and 48 GPIO lines Method: I–V with CBM	Instrumentation amplifier AD620BNZ with shunt resistor	-	Instrumentation amplifier AD620BNZ as attenuator	-	Instrumentation amplifier AD620BNZ	-	PT100	-	Based on shunted PV	-	Natural light	A: Inside/ Outside; B: Average/ Long; C: Average; D: Low.
Cotfas [80]	PC with NI NELVIS II, NI myDAQ or NI myRIO and RELab board	LabVIEW Method: I–V with CBM	NI platform with instrumentation amplifier AD8222 with shunt resistor	-	NI platform with Instrumentation amplifier AD8222	-	NI platform with	-	LM35	±0.25 °C	TSL230	±10%	Halogen lamp or natural light	A: Inside/ Outside; B: Short; C: Average; D: Average.

Table 1. *Cont.*

Reference	Platform and Method		Current		Voltage		Temperature		Temp. Sensors		Irradiance		Testing Conditions/ Comments	Application Scope [4]
	Device	Characteristics	Device	Ch. [1]	Device	Ch. [1]	Device	Ch. [1]	Device	Ch. [1]	Device	Ch. [1]		
Hybrid system														
Chen et al. [83]	TMS320F28335 DSP processor	LabVIEW Method: I–V with CBM	LTS 15-NP	Accuracy, 0.7% (Datasheet)	LV 25-P	Accuracy, 0.9% (Datasheet)	Are not mentioned	-	Are not mentioned	-	Are not mentioned	-	-	A: Inside/ Outside; B: Average/ Long; C: Average; D: Low.
Sarikh et al. [77]	Raspberry Pi	Method: I–V with TBM	ADS1115 ADC and AC712 Hall effect sensor	Comparison with a references Rsquared = 0.97793 RMSE = 0.35678 MSE = 0.034203	ADS1115 ADC and voltage resistive divider	Comparison with a reference Rsquared = 0.98567 RMSE = 1.0779 MSE = −0.01777	ADS1115 ADC	-	Pt-1000 RTD	-	ADS1115 ADC and shunted solar cell	-	Simulation and natural light	A: Inside/ Outside; B: Average/ Long; C: Average; D: Low.
García-Valverde et al. [85]	PC and TM4C123G evaluation board	LabVIEW Method: I–V with CBM	12-bit ADC with TS912BIDT OpAmp and LR2512-R50FW shunt resistance	-	12-bit ADC with TS912BIDT OpAmp and 300.2-100M-DF-1:1000-DF voltage divider	-	Arduino Mega 2560 R3 with	-	DS18B20 and DHT22 (temperature and humidity) sensors	-	BPW34 Photodiode	-	Natural light	A: Outside; B: Short/ Average; C: Average; D: Low.
Shapsough et al. [86]	Raspberry Pi	IoT concept Method: I–V with CBM	Yocotwatt wattmeter	Sample rate, 100 Hz	Yocotwatt wattmeter	Sample rate, 100 Hz	Are not mentioned	-	Are not mentioned	-	Are not mentioned	-	Natural light	A: Outside; B: Long; C: Average; D: Average.
Pereira et al. [87]	Raspberry Pi	IoT concept Method: monitoring only	SanUSB microcontroller+ ACS712—5A sensor	1.5% error	SanUSB microcontroller + voltage resistive divider		SanUSB microcontroller and Raspberry Pi	-	LM35 and DHT11	Accuracy 0.5 °C and accuracy 2 °C for temperature and 5% for humidity	LP02 Pyranometer with SanUSB microcontroller and LM324 amplifier	-	Natural light	A: Outside; B: Long; C: Low/ Average; D: Low.
TEG Component Alone														
Carmo et al. [63]	PC	LabVIEW	Agilent 34410A with $6\frac{1}{2}$ digits	Max. error: {40 µA, 60 µA, 0.6 mA} for the range of {100 mA, 1 A, 3 A}	Agilent 34410A with $6\frac{1}{2}$ digits	Max. error: {3 µV, 6 µV, 40 µV} for the range of {100 mV, 1 V, 10 V}	PC and NI USB-6009	-	Two thermistors	-	Typical quantity -	-	Laboratory design system/ Tested TEG-TEC1 -12707	A: Inside; B: Short; C: Average/ High; D: Average/ High.

Table 1. *Cont.*

Reference	Platform and Method		Current		Voltage		Temperature		Temp. Sensors		Irradiance		Testing Conditions/ Comments	Application Scope [4]
	Device	Characteristics	Device	Ch. [1]	Device	Ch. [1]	Device	Ch. [1]	Device	Ch. [1]	Device	Ch. [1]		
Hybrid system														
Izidoro et al. [68]	PC + PIC18F452 microcontroller	-	PIC18F452 microcontroller + ACS712-5 sensor	Errors with calibration: 2%	PIC18F452 microcontroller + voltage resistive divider	Errors with calibration: ±1.5%	MAX31855	Errors with calibration: 5%	K-type thermocouples	Included in the system error	-	-	Laboratory design system/ Tested TEG—inbC1-127.08HTS	A: Inside; B: Short; C: Average/ High; D: Average/ High.
Massaguer et al. [69]	PC NI cRIO	-	NI cRIO + I/O module (type is not specified)	-	NI cRIO + I/O module (type is not specified)	-	NI cRIO + I/O module (type is not specified)	-	K-type thermocouples	-	-	-	Laboratory design system	A: Inside; B: Short/ Average; C: High; D: High.
Al Musleh et al. in [70]	PC	-	RO2—I-V TRACER	Accuracy, 1.5%	RO2—I-V TRACER	Accuracy, 1.5%	WL 110 heat exchanger unit	-	RTD PT100—type JUMO 902150/10	Accuracy ± 0.12%= ±0.24 °C	Paddle-wheel water flow meter type Bürkert 783724Y	±2% of full scale = ±0.083 l/m	Laboratory design system/ Tested TEG—GM250-127 –14-16 (European Thermodynamics Limited)	A: Inside; B: Short/ Average; C: High; D: High.

[1] Ch = Characteristics (error, accuracy and uncertainty), [2] Measurement accuracy during the test, [3] Maximum standard uncertainty, [4] see the application scope list from Section 4.2.

Table 2. Software and methods for numerical analysis of HS.

Ref	Software	HS Type	Comments
Koushik et al. [35]	MATLAB-Simulink	directly coupled HS	
Shatar et al. [36]	MATLAB-Simulink	directly coupled HS	agriculture application
Keser et al. [37]	MS Visio—Visio OTK with thermal solver Sinda	directly coupled HS	space application/finite volume method
Teffah et al. [38]	MATLAB-Simulink and COMSOL Multiphysics	directly coupled HS	finite element model
Kolahan et al. [39]	FORTRAN		tridiagonal matrix algorithm
Gu et al. [19]	MATLAB	directly coupled HS	finite element model
Skjølstrup and Søndergaard [40]	MATLAB	indirectly coupled HS	Nelder–Mead simplex algorithm
Mohammadnia et al. [43] and [44]	Engineering Equation Solver	indirectly coupled HS	CPV/Stirling engine/TEG
Salari in [45]	-	directly coupled HS	finite volume method
Mahmoudinezhad et al. [47]	MATLAB	directly coupled HS	finite volume method
Mahmoudinezhad et al. [48]	COMSOL Multiphysics	directly coupled HS	3-diode finite element analysis
Shittu et al. [46]	COMSOL Multiphysics	indirectly coupled HS	3-diode finite element method
Riahi et al. [57]	Engineering Equation Solver	directly coupled HS	CPVT-TEG/energy balance equations
Zhou et al. [58]	MATLAB	directly coupled HS	
Massaguer et al. [69]	TRNSYS and Fortran	TEG only	finite differences and Newton–Raphson
Al Musleh et al. [70]	COMSOL Multiphysics V5.4	TEG only	finite element method

Author Contributions: Conceptualization, P.A.C. and D.T.C.; methodology, P.A.C.; investigation, P.A.C. and D.T.C.; resources, P.A.C. and D.T.C.; writing—original draft preparation, P.A.C.; writing—review and editing, D.T.C.; visualization, P.A.C.; project administration, D.T.C. All authors have read and agreed to the published version of the manuscript.

Funding: This research received no external funding.

Conflicts of Interest: The authors declare no conflict of interest.

References

1. REN21. Renewables 2019 Global Status Report Collaborative. Edited by Lisa Mastny and James Glave. Ren21. Vol. 105. REN21 Secretariat, Paris, France. 2019. Available online: https://www.ren21.net/wp-content/uploads/2019/05/gsr_2019_full_report_en.pdf (accessed on 15 November 2020).
2. Green, M.A.; Dunlop, E.D.; Hohl-Ebinger, J.; Yoshita, M.; Kopidakis, N.; Ho-Baillie, A.W.Y. Solar cell efficiency tables (Version 55). *Prog. Photovolt. Res. Appl.* **2020**, *28*, 3–15. [CrossRef]
3. Cotfas, D.T.; Cotfas, P.A. Multiconcept methods to enhance photovoltaic system efficiency. *Int. J. Photoenergy* **2019**, *2019*. [CrossRef]
4. Grubišić Čabo, F.; Nižetić, S.; Giama, E.; Papadopoulos, A. Techno-economic and environmental evaluation of passive cooled photovoltaic systems in Mediterranean climate conditions. *Appl. Therm. Eng.* **2020**, *169*, 114947. [CrossRef]
5. Nižetić, S.; Marinić-Kragić, I.; Grubišić-Čabo, F.; Papadopoulos, A.M.; Xie, G. Analysis of novel passive cooling strategies for free-standing silicon photovoltaic panels. *J. Therm. Anal. Calorim.* **2020**, *141*, 163–175. [CrossRef]
6. Joshi, S.S.; Dhoble, A.S. Photovoltaic-Thermal systems (PVT): Technology review and future trends. *Renew. Sustain. Energy Rev.* **2018**, *92*, 848–882. [CrossRef]
7. Benghanem, M.; Al-Mashraqi, A.A.; Daffallah, K.O. Performance of solar cells using thermoelectric module in hot sites. *Renew. Energy* **2016**, *89*, 51–59. [CrossRef]
8. Champier, D. Thermoelectric generators: A review of applications. *Energy Convers. Manag.* **2017**, *140*, 167–181. [CrossRef]
9. Pourkiaei, S.M.; Ahmadi, M.H.; Sadeghzadeh, M.; Moosavi, S.; Pourfayaz, F.; Chen, L.; Pour Yazdi, M.A.; Kumar, R. Thermoelectric cooler and thermoelectric generator devices: A review of present and potential applications, modeling and materials. *Energy* **2019**, *186*, 115849. [CrossRef]
10. Shittu, S.; Li, G.; Zhao, X.; Ma, X. Review of thermoelectric geometry and structure optimization for performance enhancement. *Appl. Energy* **2020**, *268*, 115075. [CrossRef]
11. Ma, Z.; Wei, J.; Song, P.; Zhang, M.; Yang, L.; Ma, J.; Liu, W.; Yang, F.; Wang, X. Review of experimental approaches for improving zT of thermoelectric materials. *Mater. Sci. Semicond. Process.* **2021**, *121*, 105303. [CrossRef]
12. Karthick, K.; Suresh, S.; Hussain, M.M.M.D.; Ali, H.M.; Kumar, C.S.S. Evaluation of solar thermal system configurations for thermoelectric generator applications: A critical review. *Sol. Energy* **2019**, *188*, 111–142. [CrossRef]
13. Sahin, A.Z.; Ismaila, K.G.; Yilbas, B.S.; Al-Sharafi, A. A review on the performance of photovoltaic/thermoelectric hybrid generators. *Int. J. Energy Res.* **2020**, *44*, 3365–3394. [CrossRef]
14. Shittu, S.; Li, G.; Akhlaghi, Y.G.; Ma, X.; Zhao, X.; Ayodele, E. Advancements in thermoelectric generators for enhanced hybrid photovoltaic system performance. *Renew. Sustain. Energy Rev.* **2019**, *109*, 24–54. [CrossRef]
15. Babu, C.; Ponnambalam, P. The role of thermoelectric generators in the hybrid PV/T systems: A review. *Energy Convers. Manag.* **2017**, *151*, 368–385. [CrossRef]
16. Allouhi, A. Advances on solar thermal cogeneration processes based on thermoelectric devices: A review. *Sol. Energy Mater. Sol. Cells* **2019**, *200*, 109954. [CrossRef]
17. Sripadmanabhan, S.; Aravind, C.; Chong, K.; Saidur, R.; Faizal, M.; Abubakar, S.; Paiman, S. A review on various configurations of hybrid concentrator photovoltaic and thermoelectric generator system. *Sol. Energy* **2020**, *201*, 122–148. [CrossRef]
18. Kossyvakis, D.N.; Voutsinas, G.D.; Hristoforou, E.V. Experimental analysis and performance evaluation of a tandem photovoltaic-thermoelectric hybrid system. *Energy Convers. Manag.* **2016**, *117*, 490–500. [CrossRef]
19. Gu, W.; Ma, T.; Song, A.; Li, M.; Shen, L. Mathematical modelling and performance evaluation of a hybrid photovoltaic-thermoelectric system. *Energy Convers. Manag.* **2019**, *198*, 111800. [CrossRef]

20. Rajaee, F.; Rad, M.A.V.; Kasaeian, A.; Mahian, O.; Yan, W.M. Experimental analysis of a photovoltaic/thermoelectric generator using cobalt oxide nanofluid and phase change material heat sink. *Energy Convers. Manag.* **2020**, *212*, 112780. [CrossRef]
21. Makki, A.; Omer, S.; Su, Y.; Sabir, H. Numerical investigation of heat pipe-based photovoltaic-thermoelectric generator (HP-PV/TEG) hybrid system. *Energy Convers. Manag.* **2016**, *112*, 274–287. [CrossRef]
22. Shittu, S.; Li, G.; Zhao, X.; Zhou, J.; Ma, X.; Akhlaghi, Y.G. Experimental study and exergy analysis of photovoltaic-thermoelectric with flat plate micro-channel heat pipe. *Energy Convers. Manag.* **2020**, *207*, 112515. [CrossRef]
23. Li, G.; Zhao, X.; Ji, J. Conceptual development of a novel photovoltaic-thermoelectric system and preliminary economic analysis. *Energy Convers. Manag.* **2016**, *126*, 935–943. [CrossRef]
24. Cotfas, P.A.; Cotfas, D.T.; Machidon, O.M. Modelling and PSPICE Simulation of a Photovoltaic/Thermoelectric System. In Proceedings of the IEEE 22nd International Symposium for Design and Technology in Electronic Packaging, SIITME, Oradea, Romania, 20–23 October 2016.
25. Bonin, R.; Boero, D.; Chiaberge, M.; Tonoli, A. Design and characterization of small thermoelectric generators for environmental monitoring devices. *Energy Convers. Manag.* **2013**, *73*, 340–349. [CrossRef]
26. Babu, C.; Ponnambalam, P. The theoretical performance evaluation of hybrid PV-TEG system. *Energy Convers. Manag.* **2018**, *173*, 450–460. [CrossRef]
27. Rowe, D.M. *Thermoelectrics Handbook: Macro to Nano (Google eBook)*; CRC Press: Boca Raton, FL, USA, 2010; ISBN 1420038907.
28. Martins, J.; Goncalves, L.M.; Antunes, J.; Brito, F.P. Thermoelectric exhaust energy recovery with temperature control through heat pipes. *SAE Tech. Pap.* **2011**. [CrossRef]
29. Ando, O.H.; Izidoro, C.L.; Gomes, J.M.; Correia, J.H.; Carmo, J.P.; Schaeffer, L. Acquisition and monitoring system for TEG characterization. *Int. J. Distrib. Sens. Networks* **2015**, *2015*, 1–7. [CrossRef]
30. Lineykin, S.; Ben-Yaakov, S. PSPICE-Compatible Equivalent Circuit of Thermoelectric Coolers. In Proceedings of the IEEE 36th Conference on Power Electronics Specialists, Recife, Brazil, 16 June 2005; Volume 2005, pp. 608–612. [CrossRef]
31. Mahmoudinezhad, S.; Rezania, A.; Cotfas, P.A.; Cotfas, D.T.; Rosendahl, L.A. Transient behavior of concentrated solar oxide thermoelectric generator. *Energy* **2019**, *168*, 823–832. [CrossRef]
32. Turcotte, D.; Rossb, M.; Sheriffa, F. Photovoltaic Hybrid System Sizing And Simulation Tools: Status And Needs. In Proceedings of the PV Horizon: Workshop on Photovoltaic Hybrid Systems, Montreal, QC, Canada, 10 September 2001; Volume 13, pp. 1–10.
33. Sinha, S.; Chandel, S.S. Review of software tools for hybrid renewable energy systems. *Renew. Sustain. Energy Rev.* **2014**, *32*, 192–205. [CrossRef]
34. Van Sark, W.G.J.H.M. Feasibility of photovoltaic—Thermoelectric hybrid modules. *Appl. Energy* **2011**, *88*, 2785–2790. [CrossRef]
35. Koushik, S.; Das, S.; Sharma, V.; Walde, P.; Maji, N. PV and TEG Hybrid Power Generation for Enhancement of Efficiency. In Proceedings of the India International Conference on Power Electronics IICPE, Jaipur, India, 13–15 December 2018. [CrossRef]
36. Shatar, N.M.; Abdul Rahman, M.A.A.; Shaikh Salim, S.A.Z.; Ariff, M.H.M.; Muhtazaruddin, M.N.; Badlisah, A.K.A. Design of Photovoltaic-Thermoelectric Generator (PV-TEG) Hybrid System for Precision Agriculture. In Proceedings of the IEEE 7th International Conference on Power and Energy, PECon, Kuala Lumpur, Malaysia, 3–4 December 2018; pp. 50–55. [CrossRef]
37. Keser, O.F.; Idare, B.; Bulat, B.; Okan, A. The Usability of PV-TEG Hybrid Systems on Space Platforms. In Proceedings of the 9th International Conference on Recent Advances in Space Technologies, RAST, Istanbul, Turkey, 11–14 June 2019; pp. 109–115. [CrossRef]
38. Teffah, K.; Zhang, Y. Modeling and experimental research of hybrid PV-thermoelectric system for high concentrated solar energy conversion. *Sol. Energy* **2017**, *157*, 10–19. [CrossRef]
39. Kolahan, A.; Maadi, S.R.; Kazemian, A.; Schenone, C.; Ma, T. Semi-3D transient simulation of a nanofluid-base photovoltaic thermal system integrated with a thermoelectric generator. *Energy Convers. Manag.* **2020**, *220*, 113073. [CrossRef]
40. Skjølstrup, E.J.H.; Søndergaard, T. Design and optimization of spectral beamsplitter for hybrid thermoelectric-photovoltaic concentrated solar energy devices. *Sol. Energy* **2016**, *139*, 149–156. [CrossRef]

41. Yang, Z.; Li, W.; Chen, X.; Su, S.; Lin, G.; Chen, J. Maximum efficiency and parametric optimum selection of a concentrated solar spectrum splitting photovoltaic cell-thermoelectric generator system. *Energy Convers. Manag.* **2018**, *174*, 65–71. [CrossRef]
42. Yin, E.; Li, Q.; Xuan, Y. A novel optimal design method for concentration spectrum splitting photovoltaic e thermoelectric hybrid system. *Energy* **2018**, *163*, 519–532. [CrossRef]
43. Mohammadnia, A.; Ziapour, B.M. Investigation effect of a spectral beam splitter on performance of a hybrid CPV/Stirling/TEG solar power system. *Appl. Therm. Eng.* **2020**, *180*. [CrossRef]
44. Mohammadnia, A.; Rezania, A.; Ziapour, B.M.; Sedaghati, F.; Rosendahl, L. Hybrid energy harvesting system to maximize power generation from solar energy. *Energy Convers. Manag.* **2020**, *205*. [CrossRef]
45. Salari, A.; Parcheforosh, A.; Hakkaki-Fard, A.; Amadeh, A. A numerical study on a photovoltaic thermal system integrated with a thermoelectric generator module. *Renew. Energy* **2020**, *153*, 1261–1271. [CrossRef]
46. Shittu, S.; Li, G.; Zhao, X.; Akhlaghi, Y.G.; Ma, X.; Yu, M. Comparative study of a concentrated photovoltaic-thermoelectric system with and without flat plate heat pipe. *Energy Convers. Manag.* **2019**, *193*, 1–14. [CrossRef]
47. Mahmoudinezhad, S.; Rezania, A.; Cotfas, D.T.; Cotfas, P.A.; Rosendahl, L.A. Experimental and numerical investigation of hybrid concentrated photovoltaic—Thermoelectric module under low solar concentration. *Energy* **2018**, *159*, 1123–1131. [CrossRef]
48. Mahmoudinezhad, S.; Ahmadi Atouei, S.; Cotfas, P.A.; Cotfas, D.T.; Rosendahl, L.A.; Rezania, A. Experimental and numerical study on the transient behavior of multi-junction solar cell-thermoelectric generator hybrid system. *Energy Convers. Manag.* **2019**, *184*, 448–455. [CrossRef]
49. Indrasari, W.; Habiburosid; Fahdiran, R. Characterization of hybrid solar panel prototype using PV-TEG module. *AIP Conf. Proc.* **2019**, *2169*. [CrossRef]
50. Ruzaimi, A.; Shafie, S.; Hassan, W.Z.W.; Azis, N.; Ya'Acob, M.E.; Supeni, E.E. Photovoltaic Panel Temperature and Heat Distribution Analysis for Thermoelectric Generator Application. In Proceedings of the 2018 IEEE 5th International Conference on Smart Instrumentation, Measurement and Application ICSIMA, Songkla, Thailand, 28–30 November 2018; pp. 28–30. [CrossRef]
51. Shatar, N.M.; Rahman, M.A.A.; Muhtazaruddin, M.N.; Salim, S.A.Z.S.; Singh, B.; Muhammad-Sukki, F.; Bani, N.A.; Saudi, A.S.M.; Ardila-Rey, J.A. Performance evaluation of unconcentrated photovoltaic-thermoelectric generator hybrid system under tropical climate. *Sustainability* **2019**, *11*, 6192. [CrossRef]
52. Piarah, W.H.; Djafar, Z.; Syafaruddin; Mustofa. The characterization of a spectrum splitter of Techspec AOI 50.0mm square hot and cold mirrors using a halogen light for a photovoltaic-thermoelectric generator hybrid. *Energies* **2019**, *12*, 353. [CrossRef]
53. Bruzzi, M.; Baldi, A.; Carnevale, E.A.; Catelani, M.; Ciani, L. Conversion efficiency of Si-InGaAs and GaAsP-Si-Ge lateral beam splitting photovoltaic devices. *Measurement* **2018**, *119*, 102–107. [CrossRef]
54. Cotfas, D.T.; Cotfas, P.A.; Ciobanu, D.; MacHidon, O.M. Characterization of Photovoltaic-Thermoelectric-Solar Collector Hybrid Systems in Natural Sunlight Conditions. *J. Energy Eng.* **2017**, *143*. [CrossRef]
55. Popov, R.; Paunkov, N.; Rangelova, V.; Georgiev, A. Study of hybrid thermal system with photovoltaic panels using virtual instruments. *Renew. Energy* **2020**, *154*, 1053–1064. [CrossRef]
56. Lashin, A.; Turkestani, M.A.; Sabry, M. Concentrated photovoltaic/thermal hybrid system coupled with a thermoelectric generator. *Energies* **2019**, *12*, 2623. [CrossRef]
57. Riahi, A.; Ben Haj Ali, A.; Fadhel, A.; Guizani, A.; Balghouthi, M. Performance investigation of a concentrating photovoltaic thermal hybrid solar system combined with thermoelectric generators. *Energy Convers. Manag.* **2020**, *205*, 112377. [CrossRef]
58. Zhou, Y.; Yin, X.; Zhang, Q.; Wang, N.; Yamamoto, A.; Koumoto, K.; Shen, H.; Lin, H. Perovskite solar cell-thermoelectric tandem system with a high ef fi ciency of over 23%. *Mater. Today Energy* **2019**, *12*, 363–370. [CrossRef]
59. Li, G.; Shittu, S.; Zhou, K.; Zhao, X.; Ma, X. Preliminary experiment on a novel photovoltaic-thermoelectric system in summer. *Energy* **2019**, *188*, 116041. [CrossRef]
60. Ahiska, R.; Ahiska, K. New method for investigation of parameters of real thermoelectric modules. *Energy Convers. Manag.* **2010**, *51*, 338–345. [CrossRef]
61. Ahiska, R.; Dişlitaş, S. Computer controlled test system for measuring the parameters of the real thermoelectric module. *Energy Convers. Manag.* **2011**, *52*, 27–36. [CrossRef]

62. Ahiska, R.; Dislitas, S.; Omer, G. A new method and computer-controlled system for measuring the time constant of real thermoelectric modules. *Energy Convers. Manag.* **2012**, *53*, 314–321. [CrossRef]
63. Carmo, J.P.; Antunes, J.; Silva, M.F.; Ribeiro, J.F.; Goncalves, L.M.; Correia, J.H. Characterization of thermoelectric generators by measuring the load-dependence behavior. *Measurement* **2011**, *44*, 2194–2199. [CrossRef]
64. Karabetoglu, S.; Sisman, A.; Ozturk, Z.F.; Sahin, T. Characterization of a thermoelectric generator at low temperatures. *Energy Convers. Manag.* **2012**, *62*, 47–50. [CrossRef]
65. Ahiska, R.; Mamur, H. A test system and supervisory control and data acquisition application with programmable logic controller for thermoelectric generators. *Energy Convers. Manag.* **2012**, *64*, 15–22. [CrossRef]
66. Liu, C.; Chen, P.; Li, K. A 500 W low-temperature thermoelectric generator: Design and experimental study. *Int. J. Hydrogen Energy* **2014**, *39*, 15497–15505. [CrossRef]
67. Özdemir, A.E.; Köysal, Y.; Özbaş, E.; Atalay, T. The experimental design of solar heating thermoelectric generator with wind cooling chimney. *Energy Convers. Manag.* **2015**, *98*, 127–133. [CrossRef]
68. Izidoro, C.L.; Ando Junior, O.H.; Carmo, J.P.; Schaeffer, L. Characterization of thermoelectric generator for energy harvesting. *Measurement* **2017**, *106*, 283–290. [CrossRef]
69. Massaguer, E.; Massaguer, A.; Montoro, L.; Gonzalez, J.R. Development and validation of a new TRNSYS type for the simulation of thermoelectric generators. *Appl. Energy* **2014**, *134*, 65–74. [CrossRef]
70. Al Musleh, M.; Topriska, E.V.; Jenkins, D.; Owens, E. Thermoelectric generator characterization at extra-low-temperature difference for building applications in extreme hot climates: Experimental and numerical study. *Energy Build.* **2020**, *225*, 110285. [CrossRef]
71. Zhu, Y.; Xiao, W. A comprehensive review of topologies for photovoltaic I–V curve tracer. *Sol. Energy* **2020**, *196*, 346–357. [CrossRef]
72. Cotfas, D.T.; Cotfas, P.A. PV Innovative Techniques and Experimental Test Sets. In *Renewable Energy Systems: Theory, Innovations and Intelligent Applications*; Kaplanis, S., Kaplani, E., Eds.; Nova Science Publishers, Inc.: New York, NY, USA, 2013; pp. 1–28. ISBN 978-1-62417-741-5.
73. Amiry, H.; Benhmida, M.; Bendaoud, R.; Hajjaj, C.; Bounouar, S.; Yadir, S.; Raïs, K.; Sidki, M. Design and implementation of a photovoltaic I-V curve tracer: Solar modules characterization under real operating conditions. *Energy Convers. Manag.* **2018**, *169*, 206–216. [CrossRef]
74. De Medeiros, R.P.; De Macedo, E.C.T.; De Souza Neto, J.M.R.; Vitorino, M.A.; Hartmann, L.V. A simple circuit for characterization of photovoltaic module under uniform radiation and shading conditions. In Proceedings of the IEEE International Instrumentation and Measurement Technology Conference Proceedings, Taipei, Taiwan, 23–26 May 2016. [CrossRef]
75. Taciuc, M. An experimental system for measuring the PV panel characteristics curves under real operation conditions. In Proceedings of the International Symposium on Fundamentals of Electrical Engineering ISFEE, Bucharest, Romania, 30 June–2 July 2016. [CrossRef]
76. Vega, A.; Valiño, V.; Conde, E.; Ramos, A.; Reina, P. Double sweep tracer for I-V curves characterization and continuous monitoring of photovoltaic facilities. *Sol. Energy* **2019**, *190*, 622–629. [CrossRef]
77. Sarikh, S.; Raoufi, M.; Bennouna, A.; Benlarabi, A.; Ikken, B. Implementation of a plug and play I-V curve tracer dedicated to characterization and diagnosis of PV modules under real operating conditions. *Energy Convers. Manag.* **2020**, *209*, 112613. [CrossRef]
78. Cáceres, M.; Firman, A.; Montes-Romero, J.; González Mayans, A.R.; Vera, L.H.; Fernández, E.F.; de la Casa Higueras, J. Low-Cost I–V Tracer for PV Modules under Real Operating Conditions. *Energies* **2020**, *13*, 4320. [CrossRef]
79. Erkaya, Y.; Moses, P.; Marsillac, S. On-site characterization of PV modules using a portable, MOSFET-based capacitive load. In Proceedings of the IEEE 44th Photovoltaic Specialist Conference PVSC, Washington, DC, USA, 25–30 June 2017; pp. 1–4. [CrossRef]
80. Cotfas, P.A.; Cotfas, D.T. Design and implementation of RELab system to study the solar and wind energy. *Measurement* **2016**, *93*. [CrossRef]
81. Cotfas, D.T.; Cotfas, P.A.; Ursutiu, D.; Samoila, C. Current-voltage characteristic raising techniques for solar cells. Comparisons and applications. In Proceedings of the International Conference on Optimization of Electrical and Electronic Equipment, OPTIM, Brasov, Romania, 20–22 May 2010.
82. Cotfas, D.T.; Cotfas, P.A.; Floroian, D.I.; Floroian, L. Accelerated Life Test for Photovoltaic Cells Using Concentrated Light. *Int. J. Photoenergy* **2016**, *2016*. [CrossRef]

83. Chen, Z.; Lin, W.; Wu, L.; Long, C.; Lin, P.; Cheng, S. A capacitor based fast I-V characteristics tester for photovoltaic arrays. *Energy Procedia* **2018**, *145*, 381–387. [CrossRef]
84. Ortega, E.; Aranguren, G.; Jimeno, J.C. New monitoring method to characterize individual modules in large photovoltaic systems. *Sol. Energy* **2019**, *193*, 906–914. [CrossRef]
85. García-Valverde, R.; Chaouki-Almagro, S.; Corazza, M.; Espinosa, N.; Hösel, M.; Søndergaard, R.R.; Jørgensen, M.; Villarejo, J.A.; Krebs, F.C. Portable and wireless IV-curve tracer for >5 kV organic photovoltaic modules. *Sol. Energy Mater. Sol. Cells* **2016**, *151*, 60–65. [CrossRef]
86. Shapsough, S.; Takrouri, M.; Dhaouadi, R.; Zualkernan, I. An IoT-based remote IV tracing system for analysis of city-wide solar power facilities. *Sustain. Cities Soc.* **2020**, *57*, 102041. [CrossRef]
87. Pereira, R.I.S.; Dupont, I.M.; Carvalho, P.C.M.; Jucá, S.C.S. IoT embedded linux system based on Raspberry Pi applied to real-time cloud monitoring of a decentralized photovoltaic plant. *Measurement* **2018**, *114*, 286–297. [CrossRef]
88. Pereira, R.I.S.; Jucá, S.C.S.; Carvalho, P.C.M. IoT embedded systems network and sensors signal conditioning applied to decentralized photovoltaic plants. *Measurement* **2019**, *142*, 195–212. [CrossRef]
89. Kekre, A. Solar Photovoltaic Remote Monitoring System Using IOT. In Proceedings of the International Conference on Recent Innovations in Signal Processing and Embedded Systems (RISE), Bhopal, India, 27–29 October 2017.
90. López-Vargas, A.; Fuentes, M.; Vivar, M. On the application of IoT for real-time monitoring of small stand-alone PV systems: Results from a new smart datalogger. In Proceedings of the IEEE 7th World Conference on Photovoltaic Energy Conversion (WCPEC) (A Joint Conference of 45th IEEE PVSC, 28th PVSEC & 34th EU PVSEC), Waikoloa Village, HI, USA, 10–15 June 2018.
91. Data, B.; Khan, M.S.; Delhi, N.; Sharma, H.; Haque, A.; Delhi, N. IoT Enabled Real-Time Energy Monitoring for Photovoltaic Systems. In Proceedings of the International Conference on Machine Learning, Big Data, Cloud and Parallel Computing (COMITCon), Faridabad, India, 14–16 February 2019; pp. 10–14.
92. Kumar, N.M.; Atluri, K.; Palaparthi, S. Internet of Things (IoT) in Photovoltaic Systems. In Proceedings of the National Power Engineering Conference NPEC, Madurai, India, 9–10 March 2018. [CrossRef]
93. Rouibah, N.; Barazane, L.; Mellit, A.; Hajji, B.; Rabhi, A. A Low-Cost Monitoring System for Maximum Power Point of a Photovoltaic System Using IoT Technique. In Proceedings of the International Conference on Wireless Technologies, Embedded and Intelligent Systems (WITS), Fez, Morocco, 3–4 April 2019; pp. 4–8.
94. Choi, C.; Jeong, J.; Han, J.; Park, W.; Lee, I. Implementation of IoT based PV Monitoring System with Message Queuing Telemetry Transfer protocol and Smart Utility Network. In Proceedings of the International Conference on Information and Communication Technology Convergence (ICTC), Jeju Island, Korea, 18–20 October 2017; pp. 1077–1079.
95. Choi, C.; Jeong, J.; Lee, I.; Park, W. LoRa based Renewable Energy Monitoring System with Open IoT Platform 2. LoRa based Energy IoT Monitoring. In Proceedings of the International Conference on Electronics, Information, and Communication (ICEIC), Honoulul, HI, USA, 24–27 January 2018.
96. Hamied, A. IoT-Based Experimental Prototype for Monitoring of Photovoltaic Arrays. In Proceedings of the International Conference on Applied Smart Systems (ICASS), Medea, Algeria, 24–25 November 2018.
97. Deshmukh, N.S. A Smart Solar Photovoltaic Remote Monitoring and Controlling. In Proceedings of the 2nd International Conference on Intelligent Computing and Control Systems (ICICCS), Madurai, India, 14–15 June 2018; pp. 67–71.
98. Ziolkowski, P.; Blaschkewitz, P.; Müller, E. Heat flow measurement as a key to standardization of thermoelectric generator module metrology: A comparison of reference and absolute techniques. *Measurement* **2021**, *167*, 108273. [CrossRef]
99. Guarnieri Calò Carducci, C.; Spadavecchia, M.; Attivissimo, F. High accuracy testbed for thermoelectric module characterization. *Energy Convers. Manag.* **2020**, *223*, 113325. [CrossRef]
100. Attivissimo, F.; Carducci, C.G.C.; Lanzolla, A.M.L.; Spadavecchia, M. An extensive unified thermo-electric module characterization method. *Sensors* **2016**, *16*, 2114. [CrossRef]